



# A Review of Discrete Element Method (DEM) Particle Shapes and Size Distributions for Lunar Soil

*John E. Lane*  
*ASRC Aerospace, Kennedy Space Center, Florida*

*Philip T. Metzger*  
*Kennedy Space Center, Kennedy Space Center, Florida*

*R. Allen Wilkinson*  
*Glenn Research Center, Cleveland, Ohio*

## NASA STI Program . . . in Profile

Since its founding, NASA has been dedicated to the advancement of aeronautics and space science. The NASA Scientific and Technical Information (STI) program plays a key part in helping NASA maintain this important role.

The NASA STI Program operates under the auspices of the Agency Chief Information Officer. It collects, organizes, provides for archiving, and disseminates NASA's STI. The NASA STI program provides access to the NASA Aeronautics and Space Database and its public interface, the NASA Technical Reports Server, thus providing one of the largest collections of aeronautical and space science STI in the world. Results are published in both non-NASA channels and by NASA in the NASA STI Report Series, which includes the following report types:

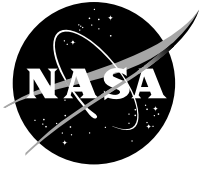
- **TECHNICAL PUBLICATION.** Reports of completed research or a major significant phase of research that present the results of NASA programs and include extensive data or theoretical analysis. Includes compilations of significant scientific and technical data and information deemed to be of continuing reference value. NASA counterpart of peer-reviewed formal professional papers but has less stringent limitations on manuscript length and extent of graphic presentations.
- **TECHNICAL MEMORANDUM.** Scientific and technical findings that are preliminary or of specialized interest, e.g., quick release reports, working papers, and bibliographies that contain minimal annotation. Does not contain extensive analysis.
- **CONTRACTOR REPORT.** Scientific and technical findings by NASA-sponsored contractors and grantees.

- **CONFERENCE PUBLICATION.** Collected papers from scientific and technical conferences, symposia, seminars, or other meetings sponsored or cosponsored by NASA.
- **SPECIAL PUBLICATION.** Scientific, technical, or historical information from NASA programs, projects, and missions, often concerned with subjects having substantial public interest.
- **TECHNICAL TRANSLATION.** English-language translations of foreign scientific and technical material pertinent to NASA's mission.

Specialized services also include creating custom thesauri, building customized databases, organizing and publishing research results.

For more information about the NASA STI program, see the following:

- Access the NASA STI program home page at <http://www.sti.nasa.gov>
- E-mail your question via the Internet to [help@sti.nasa.gov](mailto:help@sti.nasa.gov)
- Fax your question to the NASA STI Help Desk at 443-757-5803
- Telephone the NASA STI Help Desk at 443-757-5802
- Write to:  
NASA Center for AeroSpace Information (CASI)  
7115 Standard Drive  
Hanover, MD 21076-1320



# A Review of Discrete Element Method (DEM) Particle Shapes and Size Distributions for Lunar Soil

*John E. Lane*  
*ASRC Aerospace, Kennedy Space Center, Florida*

*Philip T. Metzger*  
*Kennedy Space Center, Kennedy Space Center, Florida*

*R. Allen Wilkinson*  
*Glenn Research Center, Cleveland, Ohio*

National Aeronautics and  
Space Administration

Glenn Research Center  
Cleveland, Ohio 44135

Trade names and trademarks are used in this report for identification only. Their usage does not constitute an official endorsement, either expressed or implied, by the National Aeronautics and Space Administration.

*Level of Review:* This material has been technically reviewed by technical management.

Available from

NASA Center for Aerospace Information  
7115 Standard Drive  
Hanover, MD 21076-1320

National Technical Information Service  
5301 Shawnee Road  
Alexandria, VA 22312

Available electronically at <http://gltrs.grc.nasa.gov>

# **A Review of Discrete Element Method (DEM) Particle Shapes and Size Distributions for Lunar Soil**

John E. Lane  
ASRC Aerospace  
Kennedy Space Center, Florida 32899

Philip T. Metzger  
National Aeronautics and Space Administration  
Kennedy Space Center, Florida 32899

R. Allen Wilkinson  
National Aeronautics and Space Administration  
Glenn Research Center  
Cleveland, Ohio 44135

## **Summary**

This report reviews two topics that are important to discrete element method (DEM) modeling the behavior of soils (such as lunar soils): (1) methods of modeling particle shapes and (2) analytical representations of particle size distribution. These two topics are somewhat unrelated, but both are reviewed in this report as a part of ongoing efforts to develop models of lunar soil mechanics. The choice of particle shape complexity is driven primarily by opposing tradeoffs with total number of particles, computer memory, and total simulation computer processing time. Also, the choice is dependent on available DEM software capabilities. For example, PFC2D/PFC3D and EDEM support clustering of spheres; MIMES incorporates superquadric particle shapes; and BLOKS3D provides polyhedra shapes. Most commercial and custom DEM software supports some type of complex particle shape beyond the standard sphere. Convex polyhedra, clusters of spheres and single parametric particle shapes such as the ellipsoid, poly-ellipsoid, and superquadric, are all motivated by the desire to introduce asymmetry into the particle shape, as well as edges and corners, in order to better simulate actual granular particle shapes and behavior.

An empirical particle size distribution (PSD) formula is shown to fit the example desert sand data from Bagnold, using a coarse-grade exponent  $c$  and small-grade exponent  $s$ . An additional empirical parameter  $\gamma$  has been introduced to connect the two (log-log) linear fits in the small- and coarse-grade particle size regions. Note that the PSD has been defined so that the integral from size 0 to  $\infty$  is equal to 100 in units of percent. Particle size data of JSC-1a obtained from a fine particle analyzer (FPA) at NASA Kennedy Space Center is also fitted to a similar empirical PSD function in order to extract the equivalent small- and coarse-grade exponents.

## **1.0 Introduction**

The starting point with any discrete element method (DEM) software is to model grains as spheres of a specified diameter range. The spherical particle shape greatly simplifies simulations and accommodates the maximum number of particles for any given central processing unit (CPU) execution time budget. However, it is well known that simulations of most real granular assemblies, such as sand or lunar regolith, are not accurately modeled by spheres because of the rolling of contact surfaces versus the actual frictional sliding of real particle surfaces. Most researchers active in granular modeling agree that a particle shape more complex than the sphere is required to generate simulations that can match the observable properties of real granular systems (Refs. 1 to 4). Section 2.0 of this report addresses particle shape.

The particle size distribution is one of the primary factors affecting how a soil behaves mechanically. In order to model soil mechanics, it is important to start out with an understanding of the size distribution of the soil that is being modeled. Section 3.0 of this report examines analytical models that can approximate a lunar soil particle size distribution. Appendix A shows magnified images and elemental spectra of JSC-1a lunar regolith stimulant, developed by the NASA Johnson Space Center. It should be noted that particle size distributions have been measured by several methods, which do not always agree with one another because each method is measuring a different aspect of particle “size.” Therefore, these analytical functions should not necessarily be considered definitive for lunar soil or lunar simulants until further work is accomplished. Instead, these should be considered as tentative “models” of the lunar soil particle size distribution that will be refined with further research.

## 2.0 Methods of Modeling Particle Shapes

Here, Subsections 2.1 to 2.7 cover different particle constructs. Subsection 2.8 describes a contact detection scheme, given nonspherical particles. Appendix B presents a summary of particle shape types associated with various DEM software packages, comparing some of the pros and cons of each of these idealized particle characteristics.

### 2.1 Clusters of Spheres

Popular DEM software, such as that developed and marketed by the companies Itasca and DEM Solutions Ltd., make use of sphere clusters (Fig. 1). Normally, the spheres making up a sphere cluster form a rigid body where the adhesion force between spheres is set to infinity. In some cases, researchers prefer to connect the spheres using finite adhesion forces in order to model crushing and breaking of large complex granular particles.

Another variation of particles composed of sphere clusters uses overlapping spheres (Fig. 2) (Refs. 7 to 9). Even though this is the most general case of sphere clusters, it is not necessarily the most common approach because of complications caused by its implementation in most of the commercial DEM software. DEM software typically models particles using a constant mass density. If particles of equal density overlap, the density doubles. Therefore, it is often necessary to implement a careful scaling of mass density of each of the component spheres so that the final cluster density uniformity is optimized. An algorithm to adjust mass density in two dimensions is described by Ashmawy (Ref. 8).

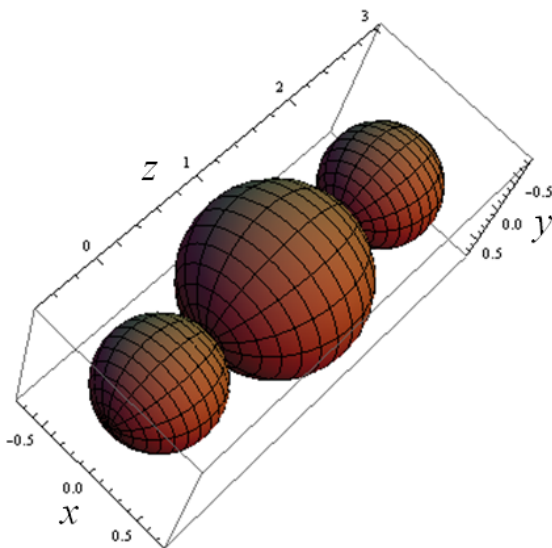


Figure 1.—Particle shape defined by cluster of nonoverlapping spheres.

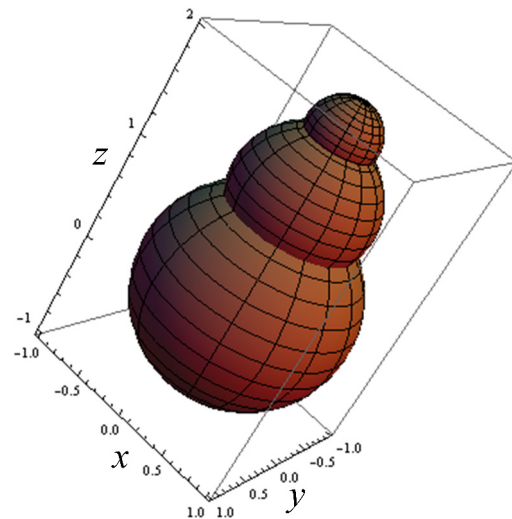


Figure 2.—Particle shape defined by cluster of overlapping spheres.

The equation of the surface a single sphere of the cluster contains in general, four parameters, the radius  $R_k$  and the vector offset  $\mathbf{r}_k = (x_k, y_k, z_k)$  relative to a local particle origin:

$$\left(\frac{x-x_k}{R_k}\right)^2 + \left(\frac{y-y_k}{R_k}\right)^2 + \left(\frac{z-z_k}{R_k}\right)^2 = 1 \quad (1)$$

For a cluster of  $N$  spheres, there will be  $1 + 4(N - 1)$  parameters since one of the spheres is defined to be centered at the origin of the local particle coordinate system. If the specific DEM software requires a mass density scaling of the component spheres, an additional parameter per sphere is needed, for a total of  $5N - 3$  parameters. If however, a density adjustment algorithm is utilized, such as that proposed by Ashmawy, only the final density of the cluster is required for a total number of parameters equal to  $4N - 2$ .

Equation (1) is valid for both overlapping and nonoverlapping clusters. A more useful representation of the surface equation is given in spherical coordinates as

$$\begin{aligned} x(\theta, \varphi) &= R_k \sin \theta \cos \varphi + x_k \\ y(\theta, \varphi) &= R_k \sin \theta \sin \varphi + y_k \\ z(\theta, \varphi) &= R_k \cos \theta + z_k \quad \text{for } 0 \leq \varphi < 2\pi, \quad 0 \leq \theta < \pi \end{aligned} \quad (2)$$

## 2.2 Ellipsoid

Other popular particle types are the two-dimensional ellipse and three-dimensional ellipsoid (Fig. 3) (Ref. 10). According to many researchers, the asymmetry provided by the ellipsoid yields the best tradeoff between particle complexity and total simulation execution time. The equation for the ellipsoid surface is similar to Equation (1):

$$\left(\frac{x}{a}\right)^2 + \left(\frac{y}{b}\right)^2 + \left(\frac{z}{c}\right)^2 = 1 \quad (3)$$

where  $a$ ,  $b$ , and  $c$  are the half-widths along each of the principal axes. The parametric form of Equation (3) is

$$\begin{aligned} x(\theta, \varphi) &= a \sin \theta \cos \varphi \\ y(\theta, \varphi) &= b \sin \theta \sin \varphi \\ z(\theta, \varphi) &= c \cos \theta \quad \text{for } 0 \leq \varphi < 2\pi, \quad 0 \leq \theta < \pi \end{aligned} \quad (4)$$

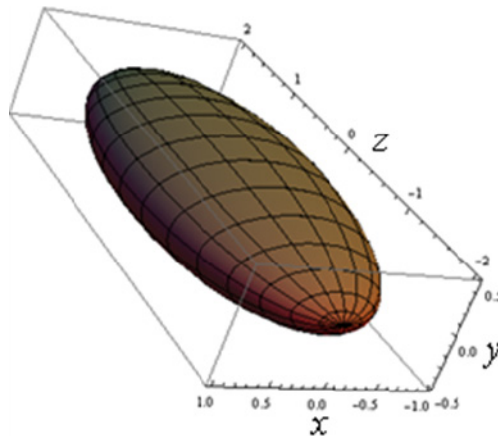


Figure 3.—Particle shape defined by an ellipsoid (Eq. (3)), with  $a = 1$ ,  $b = 0.5$ , and  $c = 2$ .

Neither the ellipse or ellipsoid lends itself to clustering strategies, since the attraction to clustering is based on a simple unit particle—the sphere. If the unit particle is an ellipse, the difficulties that arise from the ellipse tend to negate the advantages of clustering.

The ellipsoid and sphere are subsets of the superquadric shapes (Ref. 11).

### 2.3 Superquadric

The equation for the superquadric surface is similar to Equation (3):

$$\left|\frac{x}{a}\right|^K + \left|\frac{y}{b}\right|^L + \left|\frac{z}{c}\right|^M = 1 \quad (5)$$

where again  $a$ ,  $b$ , and  $c$  are the half-widths along each of the principal axes (Fig. 4). The parametric form of Equation (3) is:

$$\begin{aligned} x(\theta, \phi) &= a |\sin \theta \cos \phi|^{2/K} \operatorname{sgn}(\sin \theta \cos \phi) \\ y(\theta, \phi) &= b |\sin \theta \sin \phi|^{2/L} \operatorname{sgn}(\sin \theta \sin \phi) \\ z(\theta, \phi) &= c |\cos \theta|^{2/M} \operatorname{sgn}(\cos \theta) \end{aligned} \quad (6)$$

for  $0 \leq \phi < 2\pi$ ,  $0 \leq \theta < \pi$

where  $\operatorname{sgn}(x)$  is the sign of the argument  $x$ . The exponent parameters  $K$ ,  $L$ , and  $M$  adjust the blockiness of the shape along the three principal axis. If the exponent is less than 2, the shape becomes concave along that axis; it becomes convex for an exponent greater than or equal to 2. The superquadrics provides an additional degree of asymmetry over the ellipsoid. The greatest degree of asymmetry is achieved by defining multiple superquadric parameters in different regions. This strategy leads to the asymmetric superquadric.

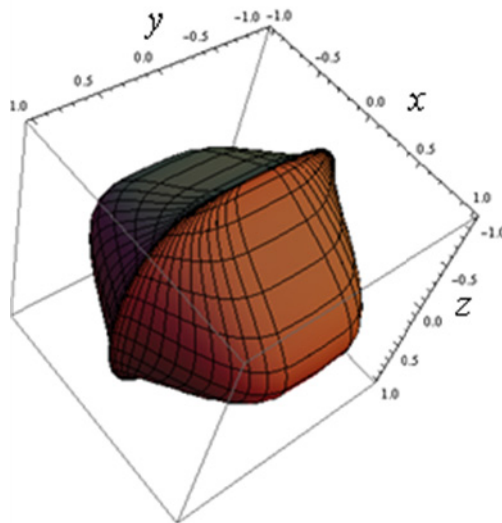


Figure 4.—Superquadric particle shape defined by Equation (5) where  $a = 1$ ,  $b = 1$ ,  $c = 1$ ,  $K = 0.6$ ,  $L = 4$ , and  $M = 2$ .

## 2.4 Asymmetric Superquadric

When Equation (6) is used with  $P$  sets of parameters in  $P$  regions, an arbitrarily asymmetric shape can be generated (Fig. 5):

$$\begin{aligned}
 x(\theta, \phi) &= \begin{cases} a_1 |\sin \theta \cos \phi|^{2/K_1} \operatorname{sgn}(\sin \theta \cos \phi) & \text{for } 0 \leq \phi < \phi_1, \quad 0 \leq \theta < \theta_1 \\ \vdots & \vdots \\ a_P |\sin \theta \cos \phi|^{2/K_P} \operatorname{sgn}(\sin \theta \cos \phi) & \text{for } \phi_{P-1} \leq \phi < 2\pi, \quad \theta_{P-1} \leq \theta < \pi \end{cases} \\
 y(\theta, \phi) &= \begin{cases} b_1 |\sin \theta \sin \phi|^{2/L_1} \operatorname{sgn}(\sin \theta \sin \phi) & \text{for } 0 \leq \phi < \phi_1, \quad 0 \leq \theta < \theta_1 \\ \vdots & \vdots \\ b_P |\sin \theta \sin \phi|^{2/L_P} \operatorname{sgn}(\sin \theta \sin \phi) & \text{for } \phi_{P-1} \leq \phi < 2\pi, \quad \theta_{P-1} \leq \theta < \pi \end{cases} \\
 z(\theta, \phi) &= \begin{cases} c_1 |\cos \theta|^{2/M_1} \operatorname{sgn}(\cos \theta) & \text{for } 0 \leq \phi < \phi_1, \quad 0 \leq \theta < \theta_1 \\ \vdots & \vdots \\ c_P |\cos \theta|^{2/M_P} \operatorname{sgn}(\cos \theta) & \text{for } \phi_{P-1} \leq \phi < 2\pi, \quad \theta_{P-1} \leq \theta < \pi \end{cases}
 \end{aligned} \tag{7}$$

For example, Figure 5 is generated by defining  $P = 2$  regions:

$$\text{Region 1: } \{0 \leq \phi < 2\pi, \quad 0 \leq \theta < \frac{1}{2}\pi\}$$

$$\text{Region 2: } \{0 \leq \phi < 2\pi, \quad \frac{1}{2}\pi \leq \theta < \pi\}$$

In the general case, the slopes are not continuous and are characterized by a sharp surface ridge.

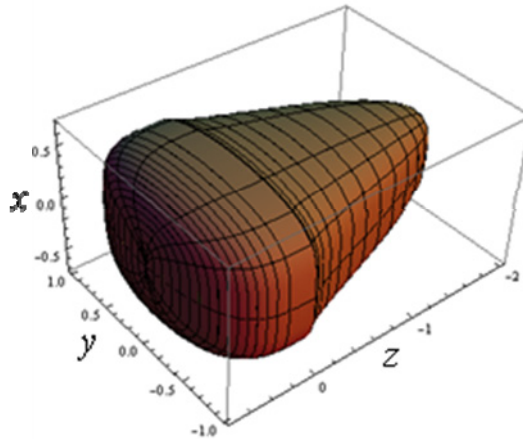


Figure 5.—Asymmetric superquadric particle shape defined by Equation (7) where  $a_1 = a_2 = 0.7$ ,  $b_1 = b_2 = 1$ ,  $c_1 = 0.75$ ,  $c_2 = 2$ ,  $K_1 = K_2 = 4$ ,  $L_1 = L_2 = 2$ ,  $M_1 = 4$ , and  $M_2 = 0.7$ .

## 2.5 Eight-Quadrant Superquadric

Defining the eight quadrants of the asymmetric superquadric as three-dimensional regions generates a useful particle shape definition:

$$\begin{aligned}
 x(\theta, \phi) &= \begin{cases} a_1 (\sin \theta \cos \phi)^{2/K_1} & \text{for } -\frac{\pi}{2} \leq \phi < \frac{\pi}{2} \\ a_2 |\sin \theta \cos \phi|^{2/K_2} & \text{for } \frac{\pi}{2} \leq \phi < \frac{3\pi}{2} \end{cases} & 0 \leq \theta < \pi \\
 y(\theta, \phi) &= \begin{cases} b_1 (\sin \theta \sin \phi)^{2/L_1} & \text{for } 0 \leq \phi < \pi \\ b_2 |\sin \theta \sin \phi|^{2/L_2} & \text{for } \pi \leq \phi < 2\pi \end{cases} & 0 \leq \theta < \pi \\
 z(\theta, \phi) &= \begin{cases} c_1 (\cos \theta)^{2/M_1} & \text{for } 0 \leq \theta < \frac{\pi}{2} \\ c_2 |\cos \theta|^{2/M_2} & \text{for } \frac{\pi}{2} \leq \theta < \pi \end{cases}
 \end{aligned} \tag{8}$$

The description of the eight-quadrant superquadric form Equation (8) is implemented in Mathematica (Ref. 12) and is shown in Figure 6, as well as in Appendix C where the eight-quadrant superquadric shape parameters are randomly modified to demonstrate the corresponding range of particle shapes.

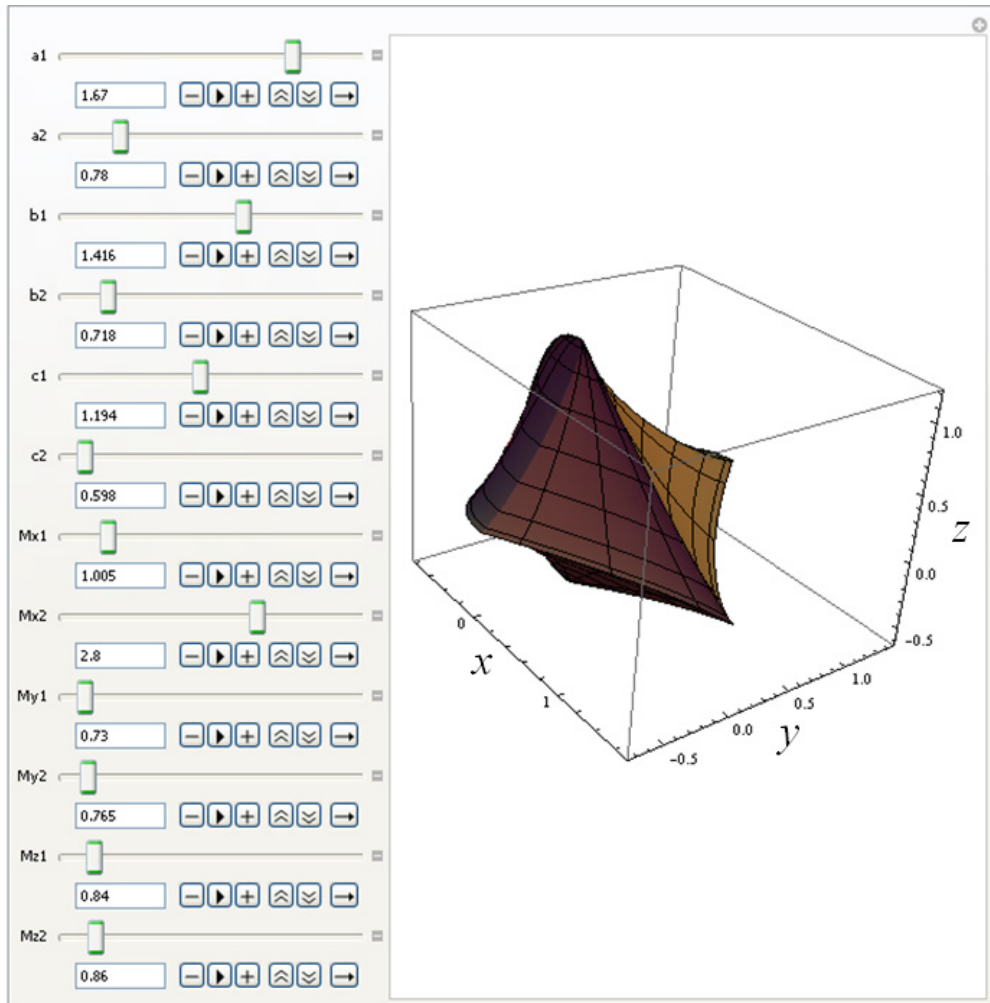


Figure 6.—Eight-quadrant superquadric video sequence using Equation (8).

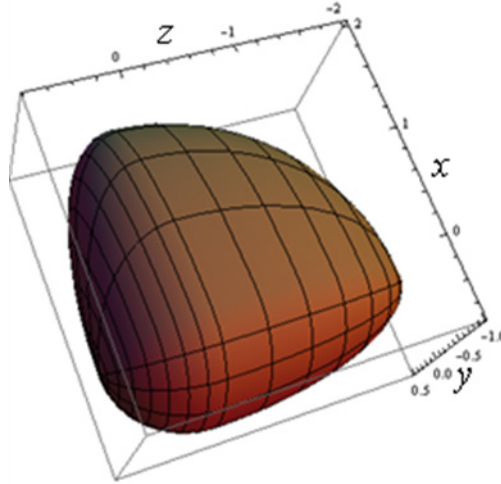


Figure 7.—Poly-ellipsoid particle shape defined by Equation (9) where  $a_1 = 2$ ,  $a_2 = 0.7$ ,  $b_1 = 0.5$ ,  $b_2 = 1$ ,  $c_1 = 0.75$ ,  $c_2 = 2$ , and  $K_1 = K_2 = L_1 = L_2 = M_1 = M_2 = 2$ .

## 2.6 Poly-Ellipsoid

Poly-ellipsoids, as defined by Peters (Ref. 13), can be viewed as a special case of the eight-quadrant superquadric discussed above. In this case (Fig. 7), there are again eight distinct regions corresponding to the eight spatial quadrants:

$$\begin{aligned}
 x(\theta, \phi) &= \begin{cases} a_1 \sin \theta \cos \phi & \text{for } -\frac{\pi}{2} \leq \phi < \frac{\pi}{2} \\ a_2 \sin \theta \cos \phi & \text{for } \frac{\pi}{2} \leq \phi < \frac{3\pi}{2} \end{cases} \\
 y(\theta, \phi) &= \begin{cases} b_1 \sin \theta \sin \phi & \text{for } 0 \leq \phi < \pi \\ b_2 \sin \theta \sin \phi & \text{for } \pi \leq \phi < 2\pi \end{cases} \\
 z(\theta, \phi) &= \begin{cases} c_1 \cos \theta & \text{for } 0 \leq \theta < \frac{\pi}{2} \\ c_2 \cos \theta & \text{for } \frac{\pi}{2} \leq \theta < \pi \end{cases}
 \end{aligned} \tag{9}$$

where, from Equation (8),  $L_1 = L_2 = M_1 = M_2 = N_1 = N_2$  are set equal to 2 only in the special case of the poly-ellipsoid. This special case defines the poly-ellipsoid and guarantees that the slopes at all quadrant boundaries are continuous.

Care must be taken in defining the parameter sets so that the surface is continuous and does not contain voids. A logical method to ensure surface continuity is accomplished by use of the poly-ellipsoid particle shape.

## 2.7 Polyhedra

All particle shapes up to this point have been described by closed-form expressions, which is a great convenience for computing first order (mass and volume) and second-order (moments of inertia) particle parameters of interest for DEM simulations, as well as computing particle interaction (contact forces). All simulated particle shapes from compound sphere clusters to poly-ellipses have one goal in common: to include shape asymmetry and sharper edges and corners for the purpose of modeling more realistic particle shapes.

A convex polyhedron can be defined by  $V$  vertices,  $E$  edges, and  $F$  faces, described conveniently by the Euler characteristic

$$V - E + F = 2 \tag{10}$$

The most convenient and compact method to define a general convex polyhedron is by a linear system of inequalities, which can be expressed in matrix form as follows:

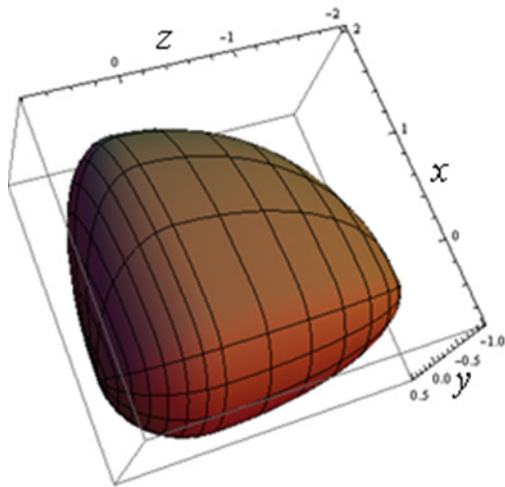
$$\mathbf{A} \cdot \mathbf{r} \leq \mathbf{b} \tag{11}$$

where  $\mathbf{r}$  is an  $N \times 1$  position vector in  $N$ -dimensional space;  $\mathbf{A}$  is an  $F \times N$  matrix ( $F$  is the number of polyhedron faces); and  $\mathbf{b}$  is an  $N \times 1$  vector.

In three-dimensional space  $\mathbf{r} = (x \ y \ z)^T$ , where  $T$  denotes “transpose.” The inequality of Equation (11) discriminates between points in the polyhedron from those outside of the surface, which are not part of the polyhedron. Replacing the inequality with an equality for each of the  $i$ th rows of  $\mathbf{A}$ , the plane of the  $i$ th face of the polyhedron is then expressed by

$$a_{i1}x + a_{i2}y + a_{i3}z - b_i = 0 \tag{12}$$

In this way, the region bounded by the intersection of all  $F$  infinite planes defined by Equation (11) defines the interior region and surface of the polyhedron. Some specific examples are shown below in Equations (13) to (16) and Figures 8 to 11.

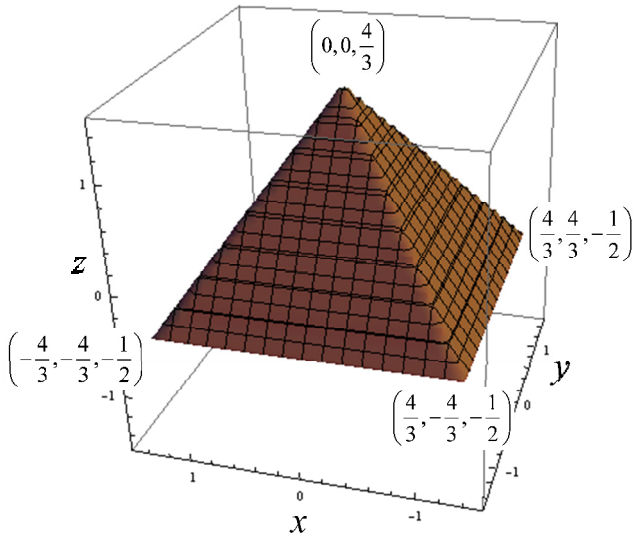


$$\mathbf{A} = \begin{pmatrix} 1 & 1 & 1 \\ 1 & -1 & -1 \\ -1 & 1 & -1 \\ -1 & -1 & 1 \end{pmatrix}$$

$$\mathbf{b} = \begin{pmatrix} 1 \\ 1 \\ 1 \\ 1 \end{pmatrix}$$

(13)

Figure 8.—Four-faced polyhedron (tetrahedron) particle shape.

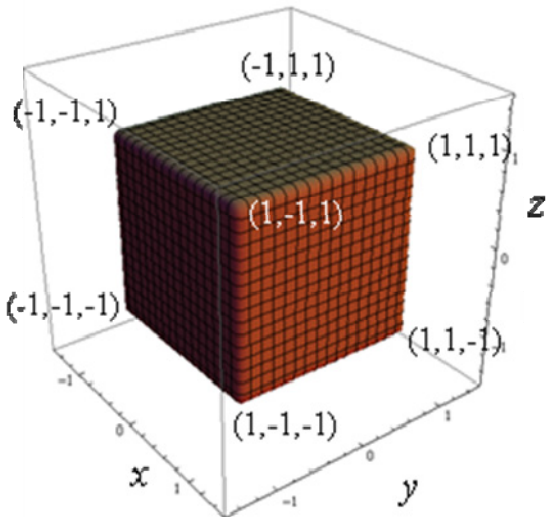


$$\mathbf{A} = \begin{pmatrix} 1 & 0 & \frac{1}{\sqrt{2}} \\ -1 & 0 & \frac{1}{\sqrt{2}} \\ 0 & 1 & \frac{1}{\sqrt{2}} \\ 0 & -1 & \frac{1}{\sqrt{2}} \\ 0 & 0 & -1 \end{pmatrix}$$

$$\mathbf{b} = \begin{pmatrix} 1 \\ 1 \\ 1 \\ 1 \\ \frac{1}{2} \end{pmatrix}$$

(14)

Figure 9.—Five-faced polyhedron (pyramid) particle shape.



$$\mathbf{A} = \begin{pmatrix} 1 & 0 & 0 \\ -1 & 0 & 0 \\ 0 & 1 & 0 \\ 0 & -1 & 0 \\ 0 & 0 & 1 \\ 0 & 0 & -1 \end{pmatrix}$$

$$\mathbf{b} = \begin{pmatrix} 1 \\ 1 \\ 1 \\ 1 \\ 1 \\ 1 \end{pmatrix}$$

(15)

Figure 10.—Six-faced polyhedron (cube) particle shape.

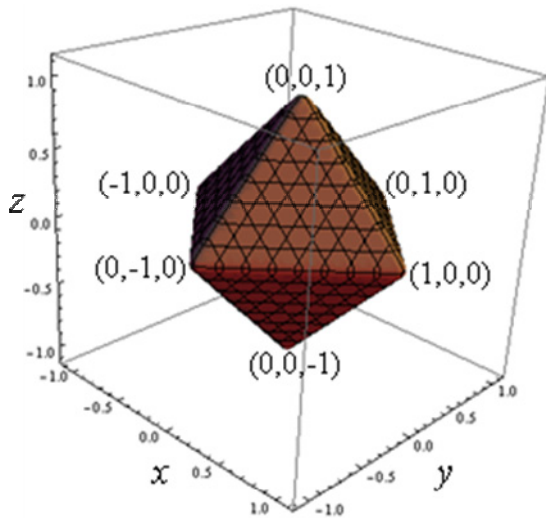


Figure 11.—Eight-faced polyhedron (octahedron) particle shape.

$$\mathbf{A} = \begin{pmatrix} 1 & 1 & 1 \\ 1 & 1 & -1 \\ 1 & -1 & 1 \\ 1 & -1 & -1 \\ -1 & 1 & 1 \\ -1 & 1 & -1 \\ -1 & -1 & 1 \\ -1 & -1 & -1 \end{pmatrix}$$

$$\mathbf{b} = \begin{pmatrix} 1 \\ 1 \\ 1 \\ 1 \\ 1 \\ 1 \\ 1 \\ 1 \end{pmatrix}$$

(16)

Simulated particle geometries based on polyhedra are a radical departure from the previous shape methodologies. General polyhedra can easily be defined with numerous faces, edges, and vertices, as well as asymmetries to closely agree with actual granular particle shapes. Traditionally, polyhedra shapes have been difficult to implement in DEM software, since the tradeoff between particle shape complexity, number of particles, memory, and CPU speed has driven most commercial DEM software towards utilizing nonpolyhedra particle shapes. Advances in computer hardware in recent years, however, has made utilization of polyhedra particles a practical strategy. The DEM software BLOKS3D developed at the University of Illinois by Zhao (Ref. 14), is an example of this strategy. Simulations using 800 particles composed of tetrahedrons (four vertices), pyramids (five vertices), cubes (eight vertices), and rhombic-dodecahedrons (14 vertices) have been reported by Zhao.

## 2.8 Contact Detection and Force Model

The most difficult parts of DEM from a CPU resources perspective are contact detection and contact force model implementation (Ref. 15). The complexity of a contact detection algorithm increases rapidly with particle shape complexity. Particle shapes that are simple spheres require the least complex detection strategy. Poly-ellipsoids, super-ellipsoids (also called superquadrics), asymmetric superquadrics, and general polyhedra require more sophisticated contact detection algorithms.

On the two extremes of contact detection algorithms, there are (1) continuous math algorithms based on analytic models of particle shape and (2) discrete math algorithms, which use gridded representations of particles. Numerous combinations of analytical and gridded algorithms, along with ad hoc algorithms, led to many possible approaches to contact detection. The details of the approach used may be intimately dependent on other unrelated aspects of the DEM code.

One method of determining the contact force direction in a continuum domain for arbitrarily shaped particles, which is loosely based on the method of Hogue (Ref. 16), makes use of the equations of the continuous particle surfaces. In this approach, two particle surfaces, described by  $f(x, y) = 0$  and  $g(x, y) = 0$ , are said to overlap when a set of coordinates can be found that simultaneously satisfy both equalities. For example, the two-dimensional case of Equation (3) defines an ellipse, so that

$$f(u, v) = 1 - \left(\frac{u}{a_1}\right)^2 - \left(\frac{v}{b_1}\right)^2 \quad g(u, v) = 1 - \left(\frac{u - u_0}{a_2}\right)^2 - \left(\frac{v - v_0}{b_2}\right)^2 \quad (17)$$

where  $u$  and  $v$  are local coordinates of the particle coordinate system. Since the particles are rotated and translated relative to the origin of the global coordinate system:

$$\begin{pmatrix} u \\ v \end{pmatrix} = \begin{pmatrix} 1 & 0 \\ 0 & 1 \end{pmatrix} \cdot \begin{pmatrix} x \\ y \end{pmatrix} \quad \text{for particle 1} \quad (18a)$$

$$\begin{pmatrix} u \\ v \end{pmatrix} = \begin{pmatrix} \cos \phi & \sin \phi \\ -\sin \phi & \cos \phi \end{pmatrix} \cdot \begin{pmatrix} x \\ y \end{pmatrix} \quad \text{for particle 2} \quad (18b)$$

then

$$f(x, y) = 1 - \left(\frac{x}{a_1}\right)^2 - \left(\frac{y}{b_1}\right)^2 \quad (19a)$$

$$g(x, y) = 1 - \left(\frac{x \cos \phi + y \sin \phi - u_0}{a_2}\right)^2 - \left(\frac{-x \cos \phi + y \sin \phi - v_0}{b_2}\right)^2 \quad (19b)$$

For this example with  $a_1 = 0.5$ ,  $b_1 = 1.1$ ,  $a_2 = 0.4$ ,  $b_2 = 1.5$ ,  $u_0 = 0.3$ ,  $v_0 = 1.8$ , and  $\phi = -30^\circ$ , the solution of the simultaneous equations  $f(x, y) = 0$  and  $g(x, y) = 0$  are

$$\begin{pmatrix} x_1 \\ y_1 \end{pmatrix} = \begin{pmatrix} 0.395809 \\ 0.672119 \end{pmatrix} \quad \begin{pmatrix} x_2 \\ y_2 \end{pmatrix} = \begin{pmatrix} 0.498069 \\ 0.0965897 \end{pmatrix} \quad (20a)$$

This case is depicted in Figure 12 where a line segment connects the two solutions. The contact force direction angle is the perpendicular to the slope of the line

$$\theta = \tan^{-1} \left( \frac{y_2 - y_1}{x_2 - x_1} \right) + \frac{\pi}{2} \quad (20b)$$

and is equal to  $10.08^\circ$  in the above case.

In general, there will be two point solutions in two dimensions and a set of solutions comprising a closed loop in three dimensions. The two-dimensional case shown in Figure 12 defines a line connecting the two points of intersection. A normal vector to this line, located at the midpoint of the line, is one method of defining an effective contact force direction as an input prelude to the contact force model. The contact force model uses the overlap area or volume information to determine the magnitude of contact repulsion.

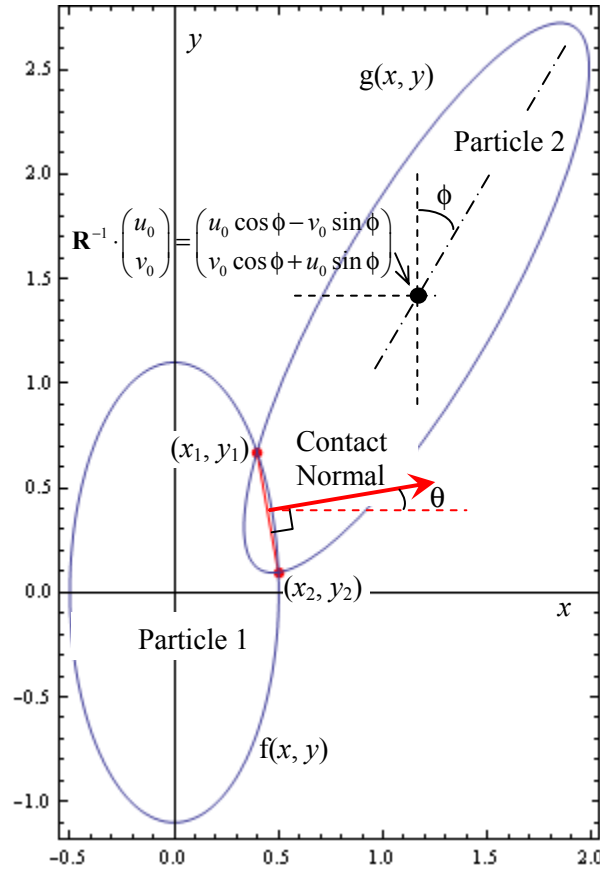


Figure 12.—Contact detection of two particles described by analytical expressions. The contact normal direction is  $\theta = 10.08^\circ$ .

In the three-dimensional case, the force direction of contacting particles is easily defined for spherical particles. Most DEM software, such as PFC3D (Ref. 5b) by Itasca, defines the force direction, in the case of simple spherical particles, as along the axis connecting contacting particle centers. In the case of more complex particles composed of clusters of overlapping spheres of different sizes, the force direction can still be modeled as along the axis connecting sphere centers of the two local spheres involved in the contact, assuming that the deformation effect due to contact can be isolated to only the two contacting spheres. In this case, the torque about the center of mass of the cluster must also be included in the equations of motion.

The details of force direction are intimately coupled to the details of the particle shape model. For example, in the shape model used by Hogue (Ref. 16), particles are made up of triangular surfaces and nodes, where the points of the triangles are nodes. When two particles contact, a node of one will usually penetrate the triangular surface of another. The force direction is defined as the normal to the triangular surface. Other possibilities include node-to-node and triangle-to-triangle contact, which are treated as special cases.

A common characteristic of most approaches to modeling contact force direction is the explicit or implicit need to know the normal to the surface of the particle at the point of contact. The gradient of the particle surface is a convenient means to quantify the surface normal of the continuous particle shape. For example, going back to the ellipsoid of Equation (3), the normal direction at any point on the surface is found from the gradient:

$$\nabla f(x, y, z) = \begin{pmatrix} \frac{\partial}{\partial x} \\ \frac{\partial}{\partial y} \\ \frac{\partial}{\partial z} \end{pmatrix} \left\{ \left( \frac{x}{a} \right)^2 + \left( \frac{y}{b} \right)^2 + \left( \frac{z}{c} \right)^2 - 1 \right\} = \begin{pmatrix} \frac{2x}{a^2} \\ \frac{2y}{b^2} \\ \frac{2z}{c^2} \end{pmatrix} \quad (21)$$

The difficulty of applying Equation (21) directly to the general case of arbitrary shaped particles is that it must be decided at what point on the contacting surface and associated normal direction is most relevant to the final contact force direction. A brute force method could involve integrating Equation (21) over the overlapping surface areas of both contacting particles to get an average normal direction, and thus a final force direction.

On the other extreme of contact detection methods, the full discrete approach to contact detection can be performed using any particle shape since once the shape has been defined, the particle location is simply designated by a cluster of pixels. As shown in Figure 13, contact detection is the simultaneous enabling of pixel bits in the quantized space of the overlapping particles. The advantage of full discrete contact detection is that there is no penalty due to particle shape. However, the obvious disadvantage is resolution of the particle states (position and velocity) in that discrete space.

The discrete version of the contact algorithm involves rectangular gridding of the particles so that any overlap can be detected and described by simultaneous occupancy of adjacent particles in one or more grids (or pixels for the two-dimensional case). Once a contact condition is detected by the overlap of one or more pixels associated with a particle pair, the direction of the contact normal can be computed by flagging the set of overlapping pixels. As is true for most mathematical models that substitute a simple solution for a more complex mathematical description, numerous approaches are possible. Below we derive (as an example) a method for calculating contact force direction that can be implemented as a computer algorithm. However we do not imply that this method is necessarily a method of choice by any specific DEM software vendor.

The set of  $M$ -occupied pixels  $\mathbf{X}_i$  can be transformed to a principal component direction by using the Hotelling transform, and then by taking the perpendicular direction, the contact normal direction can be defined. The procedure is described below.

First, the center of mass  $\mathbf{m}_x$  of the set of overlapping pixels is calculated:

$$\mathbf{m}_x = \frac{1}{M} \sum_{i=1}^M \mathbf{X}_i \quad (22)$$

Next, the centered covariance matrix is computed:

$$\mathbf{C}_x = \frac{1}{M} \sum_{i=1}^M \mathbf{X}_i \cdot \mathbf{X}_i^T - \mathbf{m}_i \cdot \mathbf{m}_i^T \quad (23)$$

The eigenvalues of  $\mathbf{C}_x$  define the principal axis directions. Adding  $90^\circ$  to the angle that defines the first principal axis defines the normal direction, which is the contact force direction.

Several commercial off-the-shelf (COTS) DEM software packages are available. In addition, several custom software packages have been developed, some of which may become COTS products in the future. In the final analysis, the choice of particle shape is predetermined by the details of specific DEM software and the particle shapes it supports. Some of these are listed in Table I.

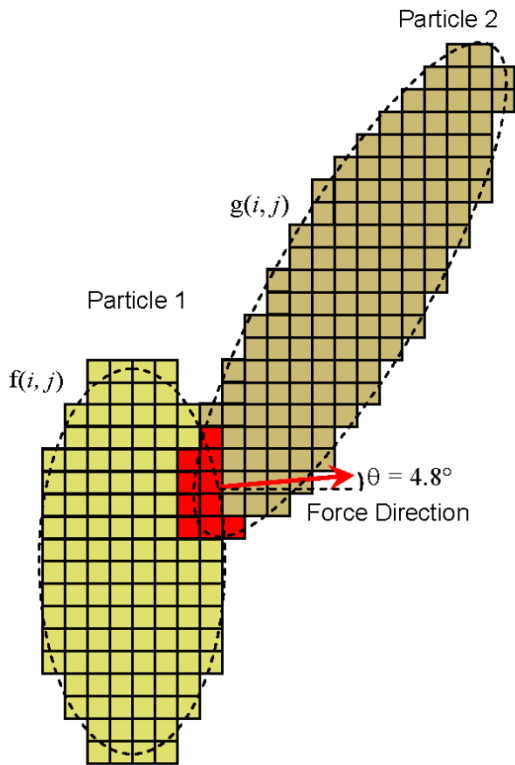


Figure 13(a).—Contact detection of two particles described by discrete particle representations with fine spatial grid.

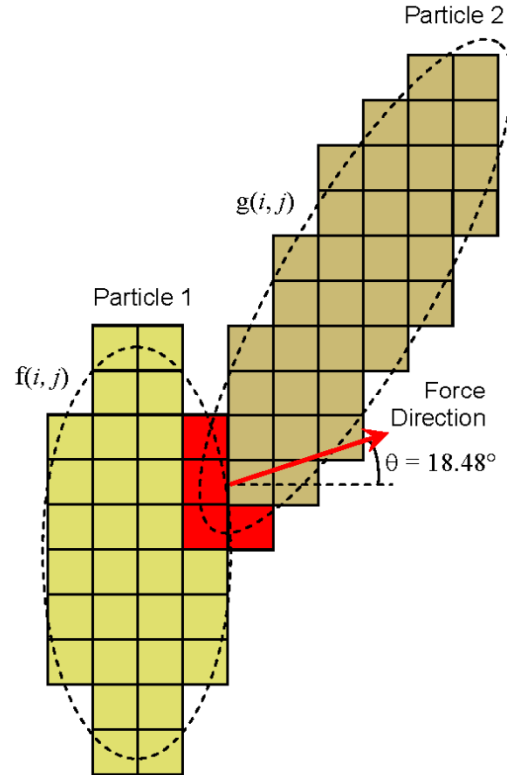


Figure 13(b).—Contact detection of two particles described by discrete particle representations with coarse spatial grid.

TABLE I.—PARTICLE SHAPE CAPABILITIES OF SOME DEM SOFTWARE

Software	Supported particle shapes
PFC2D/3D (Ref. 5)	Spheres, rigid sphere clusters: overlapping and nonoverlapping
EDEM (Ref. 6)	Spheres, sphere clusters: overlapping and nonoverlapping
BLOKS3D (Ref. 16)	Polyhedra
ROCKS3D	Polyhedra
MIMES (Ref. 17)	Superquadric shapes
YADE (Ref. 18)	Spheres Polyhedra (work in progress)

### 3.0 Analytical Representations of Particle Size Distribution

The data-fitting procedure outlined in Bagnold (Ref. 20) provides valuable insight into the nature of the desert sand particle size distribution (PSD). The technique used by Bagnold, which was appropriate for the time period, assumes that the tools of choice are a pencil, graph paper, and a ruler. Fortunately, current computer software tools are beginning to provide a reliable means to fit arbitrary nonlinear functions to a data set. Taking this approach, it makes sense to define the PSD as a single formula, covering the entire particle size range.<sup>1</sup>

<sup>1</sup>When dealing with particle size histograms and the numerous forms of size distributions and their moments, carefully keeping track of units reduces confusion and the risk of error. Also, it should be noted that histograms are summed, while distributions are integrated.

### 3.1 Size Distribution by Mass

The fractional mass of particles in a differential size increment  $dD$ , based on Bagnold's work is

$$N(D)dD = \frac{N_0}{\left((D_0/D)^{s/\gamma} + (D_0/D)^{c/\gamma}\right)^\gamma} dD \quad (24a)$$

where the small slope  $s$  is always positive and coarse slope  $c$  is always negative. The PSD of Equation (24a) is normalized by setting the integral of  $N(D)$ , for sizes from 0 to  $\infty$ , equal to 1:

$$\int_0^\infty N(D)dD = 1 \quad (24b)$$

Note that in the case of Bagnold's data, the integral is set equal to 100 percent.

For the small-diameter case,  $D \ll D_0$ , so that Equation (24a) reduces to

$$N(D) = N_0(D/D_0)^s \quad (25)$$

If Equation (25) is plotted on a log-log plot, as described by Bagnold, a straight line graph of slope  $s$  results in

$$\begin{aligned} y \equiv \log N &= \log N_0 + s \log D - s \log D_0 \\ &= y_0 + sR - sR_0 \end{aligned} \quad (26)$$

where  $R \equiv \log D$ .

In the large diameter case,  $D \gg D_0$ , so that Equation (24) reduces to

$$N(D) = N_0(D/D_0)^c \quad (27)$$

If Equation (27) is plotted on a log-log plot, a straight-line graph of slope  $c$  results, which is equivalent to

$$\begin{aligned} y \equiv \log N &= \log N_0 + c \log D - c \log D_0 \\ &= y_0 + cR - cR_0 \end{aligned} \quad (28)$$

Recall that  $c$  has been defined as negative value according to Bagnold.

The exponent parameter  $\gamma$  in Equation (24) is introduced as a means to control the transition rate between the small-diameter positive slope regime and the large-diameter negative slope regime.

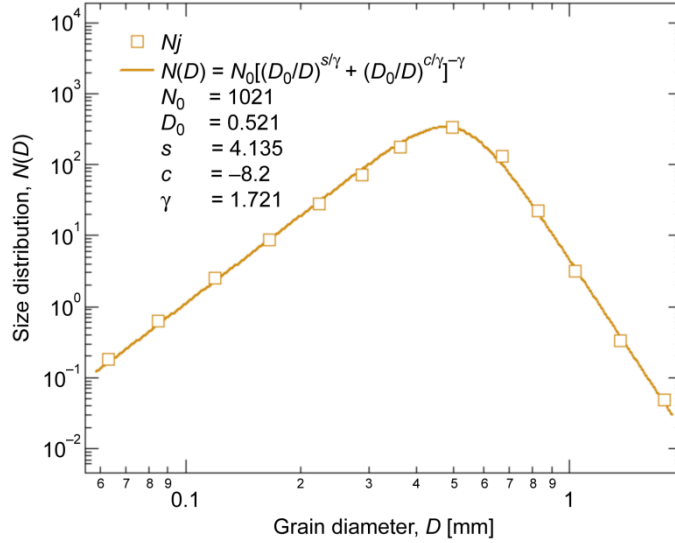


Figure 14.—Particle size distribution fit to desert sand using Equation (24a).

### 3.3 Particle Size Distribution

Equation (24) describes a size distribution based on particle mass. This formula is an empirical fit to observed grain size distributions of desert sand (Fig. 14) based on measurements using a multilevel sieve. However, the fundamental size distribution of primary interest for an assemblage of particles is  $P(D)$ , which may be expressed in units of  $[\text{m}^{-3} \text{mm}^{-1}]$ , where  $P(D)dD$  is the number of particles per unit volume of space within a differential size increment  $dD$ . The total number of particles of all sizes in a sample volume  $V_S$  is then

$$N_V = V_S \int_0^{\infty} P(D) dD \quad (29)$$

Assuming the packing density is homogeneous and repeatable, the total mass of the assemblage of particles in a volume  $V_S$  is

$$M_V = \frac{1}{6} \pi \rho V_S \int_0^{\infty} D^3 P(D) dD \quad (30)$$

where  $\rho$  is the particle grain density, assuming all grains have equal density and are spherical. Equation (30) can be rewritten in terms of the volume density of the assemblage of particles by dividing both sides by  $V_S$ :

$$\rho_V = \frac{1}{6} \pi \rho \int_0^{\infty} D^3 P(D) dD \quad (31)$$

Now the mass size distribution described by Equation (24) can be expressed in terms of  $P(D)$ :

$$\begin{aligned}
 N(D) &= \frac{\frac{1}{6} \pi \rho D^3 P(D)}{\frac{1}{6} \pi \rho \int_0^{\infty} D^3 P(D) dD} \\
 &= \frac{1}{6} \pi D^3 P(D) \frac{\rho}{\rho_V}
 \end{aligned}
 \tag{32}$$

Equation (32) can now be inverted, thus providing a means to estimate the particle size distribution  $P(D)$  from the measured mass distribution  $N(D)$ :

$$\begin{aligned}
 P(D) &= \frac{\rho_V}{\frac{1}{6} \pi D^3 \rho} N(D) \\
 &= \frac{\rho_V}{\frac{1}{6} \pi D^3 \rho} \cdot \frac{N_0}{\left( (D_0/D)^{s/\gamma} + (D/D_0)^{-s/\gamma} \right)^\gamma}
 \end{aligned}
 \tag{33}$$

where the parameters  $N_0$ ,  $s$ ,  $c$ ,  $\gamma$ ,  $\rho$ , and  $\rho_V$  are determined by measurement. Note that the particle packing ratio is less than one ( $\rho_V/\rho < 1$ ), because of gaps between particles of an assemblage.

### 3.4 FPA Data of JSC-1a

Instruments that measure and count individual particles typically output a histogram count of particles in bins of equal intervals for the property of interest. This is the case with the fine particle analyzer (FPA) used to measure a sample of JSC-1a at the NASA Kennedy Space Center Granular Mechanics and Surface Systems Laboratory. An example of particle size counts from the first nine size bin intervals of an FPA measurement are shown in Table II. Each bin interval is defined by a  $\Delta D = 1/256$  [mm], shown in the first column. The second column shows counts  $C_k$  of particles that fall into the size bin centered at the equivalent spherical diameter  $D_k$  where  $k$  is the bin index.

To convert from a histogram of counts to a size distribution  $n(D)$  in units of [mm<sup>-1</sup>], the counts are divided by the bin interval,  $\Delta D$ :

$$n(D_k) \approx n_k = \frac{C_k}{\Delta D} \text{ [mm}^{-1}\text{]}
 \tag{34}$$

The third column of Table II shows  $n_k$ , the corresponding values of the number of particles in bin  $k$ , determined from the  $C_k$  and  $\Delta D = 1/256$  [mm], using Equation (34). The  $n_k$  are plotted in Figure 15, along with an empirical fit based on a sum of exponentials:

$$n(D) = D^\gamma N_1 e^{-D/D_1} + N_2 e^{-D/D_2} \text{ [mm}^{-1}\text{]}
 \tag{35}$$

TABLE II.—FPA<sup>a</sup> PARTICLE COUNT DATA FOR JSC-1a

Particle size, $D_k$ [mm]	Particle count, $C_k$	Count per size interval, $n_k = C_k/\Delta D$ [mm <sup>-1</sup> ]
0.003906	1232155	315431680
.007813	629101	161049856
.011719	676994	173310464
0.015625	659910	168936960
.019531	602111	154140416
.023438	546315	139856640
0.027344	496099	127001344
.03125	448268	114756608
.035156	403354	103258624
⋮	⋮	⋮

<sup>a</sup>FPA refers to fine particle analyzer at NASA Kennedy Space Center.

TABLE III.—FPA<sup>a</sup> MASS DATA FOR JSC-1a

Particle size $D_k$ [mm]	$TL$ ratio, thickness/length	Mass per interval, $m_k$ [g·mm <sup>-1</sup> ]
0.003906	0.30649069	0.005223
.007813	.51233492	.041281
.011719	.54465904	.162795
0.015625	0.56233665	0.392799
.019531	.57190647	.716264
.023438	.57940036	1.143148
0.027344	0.58504106	1.670413
.03125	.58960083	2.277133
.035156	.59410737	2.948024
⋮	⋮	⋮

<sup>a</sup>FPA refers to fine particle analyzer at NASA Kennedy Space Center.

Particle mass data corresponding to the counts and diameters of Table II are shown in Table III. In the second column,  $L$  is defined as the longest chord across the particle, where a chord is defined as any line segment that crosses from one part of a particle's perimeter to another part of the same perimeter; and  $T$  is defined as the longest chord of all chords that are perpendicular to  $L$ . Typically in this context  $L$  denotes particle length and  $T$ , thickness.

The size distribution is converted to mass distribution by multiplying by particle volume and particle density:

$$m(D) = \frac{1}{6} \pi D^3 \rho \frac{R_{TL}(1 + R_{TL})}{2} n(D) \text{ [g·mm}^{-1}\text{]} \quad (36)$$

where the particle density  $\rho = 2.65 \text{ [g·cm}^{-3}\text{]}$ . The geometric factor  $R_{TL}(1 + R_{TL})/2$  in Equation (36) improves the particle volume estimate using a geometric correction factor to account for the nonspherical nature of JSC-1a. The  $TL$  ratio,  $R_{TL}$  shown in Table III, is an output of the FPA data processing. Note that as  $R_{TL}$  approaches 1, the geometric correction factor also approaches 1.

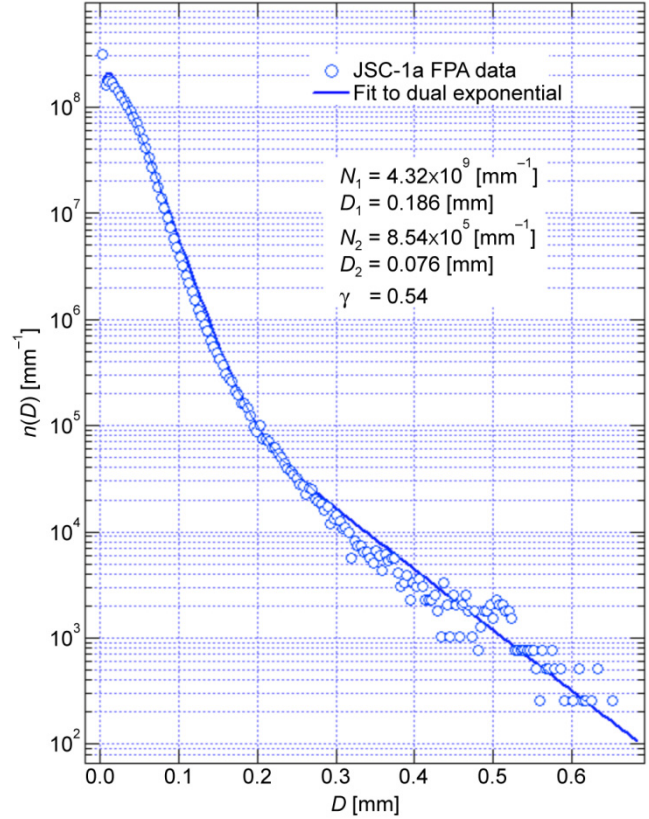


Figure 15.—Fine particle analyzer (FPA) size distribution of JSC-1a, fitted to sum of exponentials.

Using the empirical  $n(D)$  function from Equation (35) and the equation for mass shown above, the FPA particle mass data is plotted in Figure 16.

Going back to Bagnold's method, Equation (24), the particle mass data from Table III can be fitted as shown in Figure 17. In this case the parameter  $N_0$  is expressed so that  $P(D)$  from Equation (29) is in units of  $[\text{g}\cdot\text{mm}^{-1}]$ :

$$m(D) = \frac{N_0}{\left( (D_0/D)^{s/\gamma} + (D_0/D)^{c/\gamma} \right)^\gamma} [\text{g}\cdot\text{mm}^{-1}] \quad (37)$$

A small-slope parameter  $s$  and coarse-slope parameter  $c$  is determine by this fit. The FPA particle count size distribution  $n_k$  is plotted in Figure 18 along with the Bagnold's fit, found by inverting Equation (36) with  $m(D)$  from Equation (37):

$$\begin{aligned} n(D) &= \left( \frac{1}{6} \pi D^3 \rho \frac{R_{TL}(1+R_{TL})}{2} \right)^{-1} m(D) \\ &= \frac{N_0}{\left( \frac{1}{6} \pi D^3 \rho \frac{R_{TL}(1+R_{TL})}{2} \right) \left( (D_0/D)^{s/\gamma} + (D_0/D)^{c/\gamma} \right)^\gamma} [\text{mm}^{-1}] \end{aligned} \quad (38)$$

For comparison, a lognormal fit to the mass size distribution is given by

$$m(D) = \frac{m_0}{D_0} \frac{e^{-\left( \ln \frac{D}{D_0} \right)^2 / (2\sigma^2)}}{\sqrt{2\pi} \sigma (D/D_0)} [\text{g}\cdot\text{mm}^{-1}] \quad (39)$$

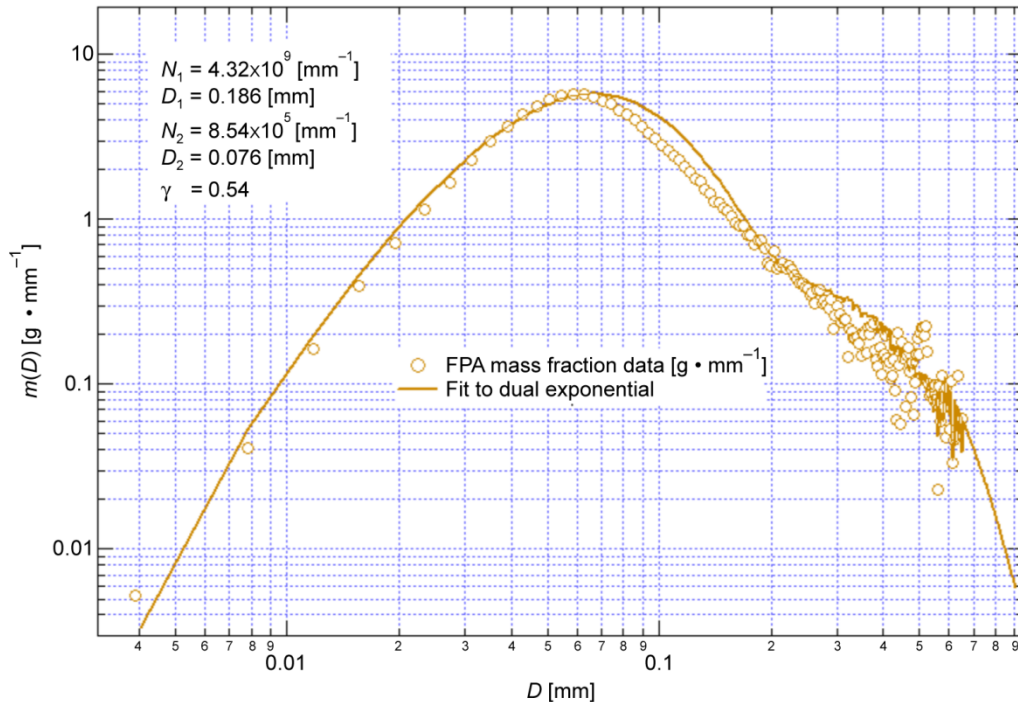


Figure 16.—Fine particle analyzer (FPA) mass size distribution of JSC-1a, fitted to sum of exponentials, Equation (35).

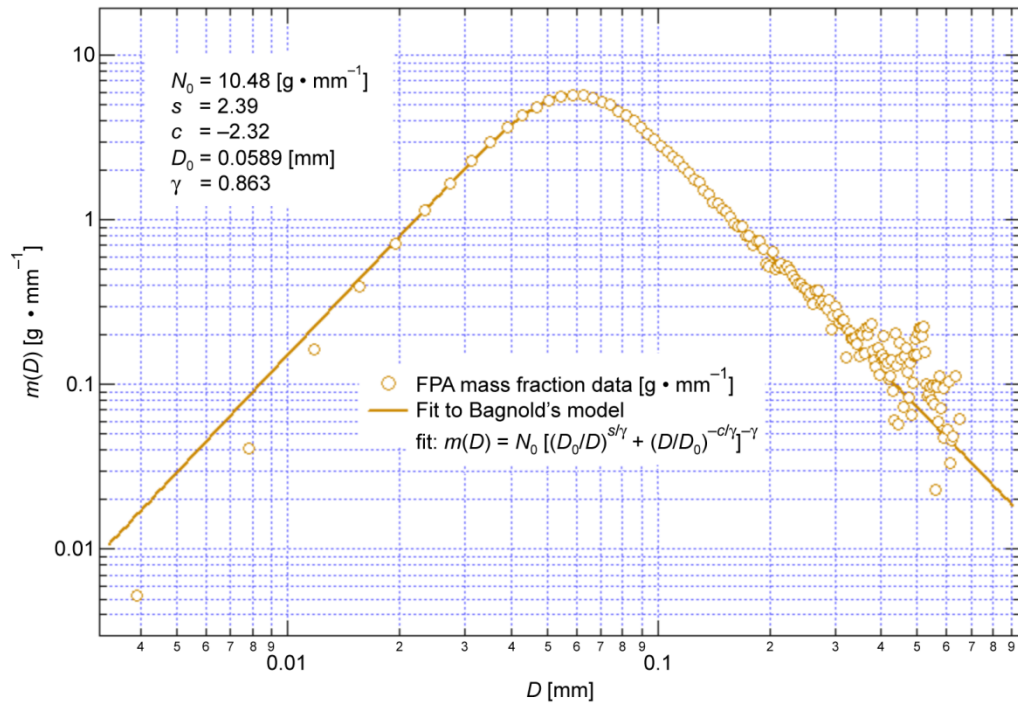


Figure 17.—Fine particle analyzer (FPA) mass size distribution of JSC-1a, fitted to Bagnold's model.

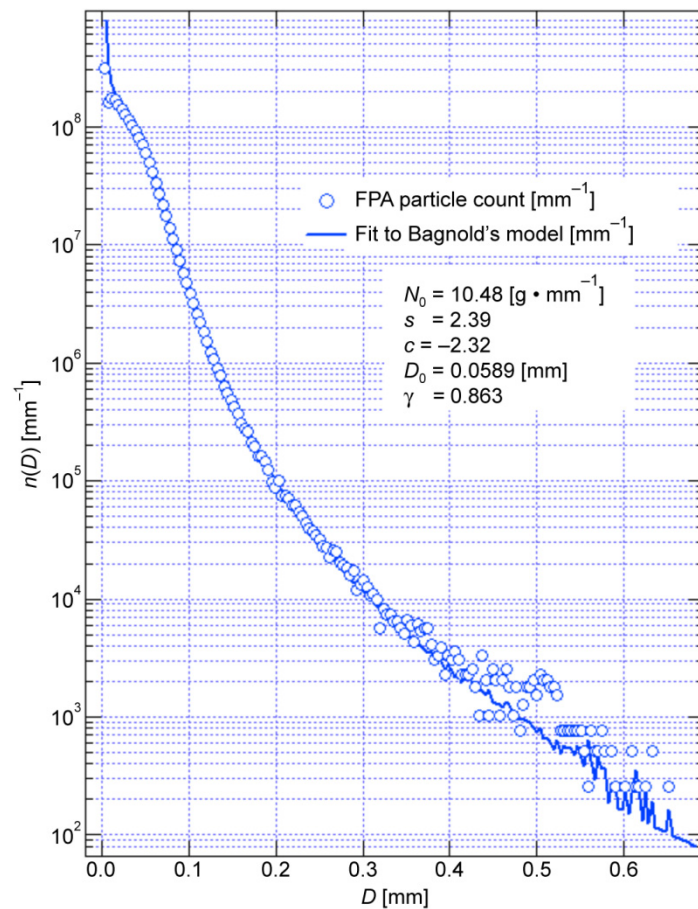


Figure 18.—Fine particle analyzer (FPA) size distribution of JSC-1a, fitted to Bagnold's model using Equation (38).

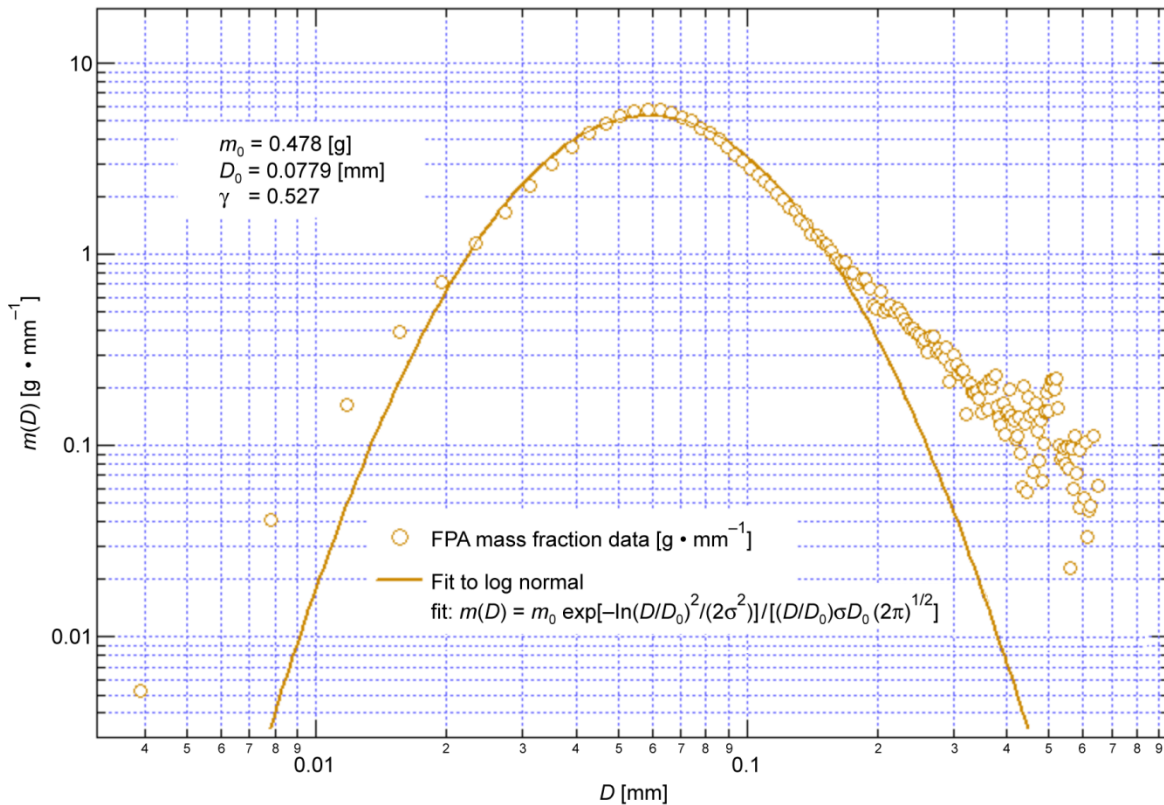


Figure 19.—Fine particle analyzer (FPA) mass size distribution of JSC-1a, fitted to lognormal distribution.

The fit of Equation (39) to JSC-1a is shown in Figure 19.

## 4.0 Concluding Remarks

This report discusses topics that are important to the modeling of the interaction and dynamics of granular particles, and in particular, lunar simulants. In Section 2.0, discrete element method (DEM) particle shapes were presented, where the choice of particle shape is motivated by many opposing tradeoffs, such as

- (1) The number of parameters describing the simulated particle surface (thus defining the interior versus exterior region). The goal is to attempt to closely match the shape of a real particle.
- (2) The total number of particles that can be incorporated in a simulation.
- (3) Computer processing resources needed: memory and total simulation time.
- (4) The difficulty versus ease of the contact detection algorithm and subsequent implementation of a force model.

Most commercial and custom DEM software supports some type of complex particle shape in order to introduce asymmetry into the particle shape, so as to better simulate real granular particles interactions and behavior.

In Section 3.0, a complete particle size distribution (PSD) formula is shown to fit the example desert sand data from Bagnold, using a coarse-grade exponent  $c$  and small-grade exponent  $s$ . An additional empirical parameter  $\gamma$  has been introduced to connect the two log-log linear fits in the small- and coarse-grade particle size regions. The key finding in this section is that Bagnold's model is a fair representation

of the PSD except for particles below 20  $\mu\text{m}$ , where it diverges somewhat. Also, the double exponential formulation is a fair representation of the size distribution, but the lognormal formulation is not very successful at matching the JSC-1a lunar stimulant used in this evaluation. Particle size data of JSC-1a obtained from a fine particle analyzer (FPA) at NASA Kennedy Space Center are also fitted to the PSD in order to extract equivalent small- and coarse-grade exponents. Note that the FPA data are uncorrelated quantitatively with other accepted PSD measuring tools, so there may be a bias in data that affects the quality of the PSD fit.

## Appendix A.—Microscope Image, Shadowgraphs, and SEM Spectrum of JSC-1a

JSC-1a is a lunar regolith simulant that was developed by the NASA Johnson Space Center. It is a basaltic ash with a high glass content. Figure 20 is an optical microscope image of the larger particles in a sample of JSC-1a. Figure 21 presents shadowgraphs of JSC-1a stimulant showing the variety of shapes and sizes in the mixture. Figure 22 is an elemental analysis spectrum of a sample of JSC-1a using a Joel 75000F scanning electron microscope (SEM) with energy-dispersive x-ray spectroscopy (EDS). Figure 23 contains elemental maps of the sample in Figure 22, showing K- $\alpha$  emission lines for the detected elements (K lines result when an electron transitions to the innermost K shell from a 2p orbital of the L shell).

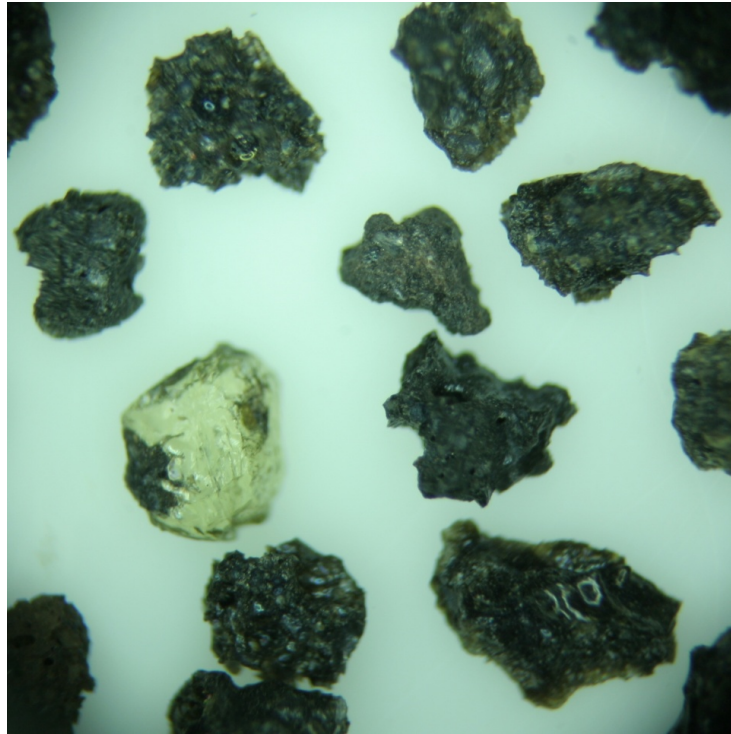


Figure 20.—Microscope image of >600- $\mu\text{m}$  particles of JCS-1a.

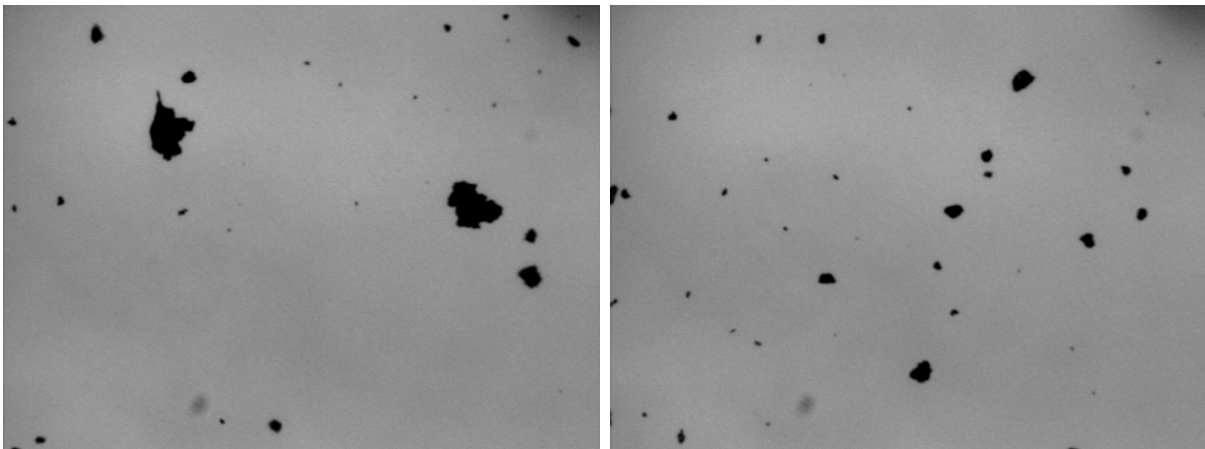
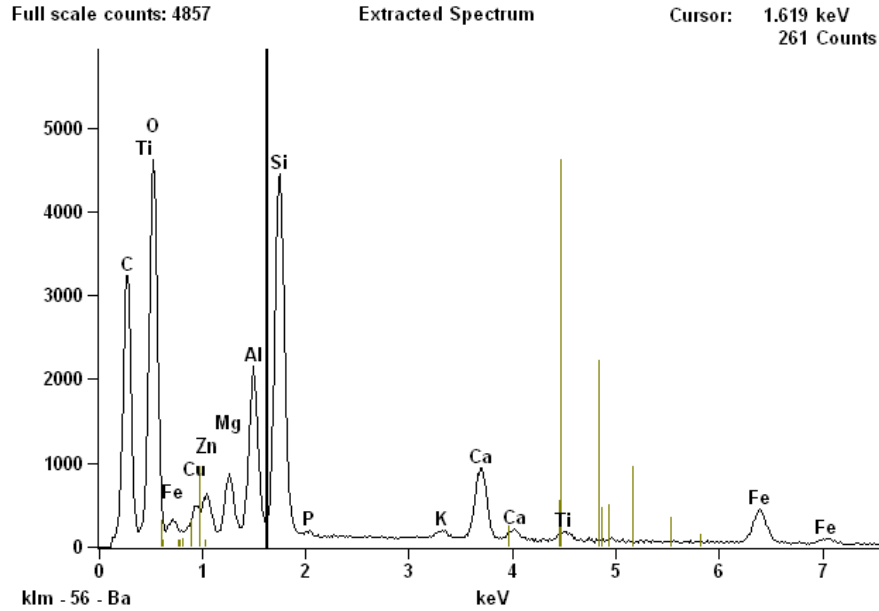


Figure 21.—Shadowgraphs of JCS-1a.



Fri Jul 11 14:09:19 2008  
 Filter Fit   Chi-squared value: 3.178   Errors: +/- 1 Sigma  
 Correction Method: Proza (Phi-Rho-Z)  
 Acc.Voltage: 15.0 kV  
 Take Off Angle: 30.0 deg

Element	Element Wt. %	Atom %
C K	48.89 +/- 0.38	61.88 +/- 0.48
O K	31.52 +/- 0.27	29.94 +/- 0.26
Mg K	0.94 +/- 0.02	0.59 +/- 0.01
Al K	2.51 +/- 0.05	1.41 +/- 0.03
Si K	5.73 +/- 0.05	3.10 +/- 0.03
P K	0.08 +/- 0.01	0.04 +/- 0.01
K K	0.23 +/- 0.01	0.09 +/- 0.01
Ca K	2.59 +/- 0.05	0.98 +/- 0.02
Ti K	0.52 +/- 0.05	0.17 +/- 0.01
Fe K	3.85 +/- 0.13	1.05 +/- 0.03
Cu K	1.93 +/- 0.20	0.46 +/- 0.05
Zn K	1.21 +/- 0.14	0.28 +/- 0.03
Total	100.00	100.0

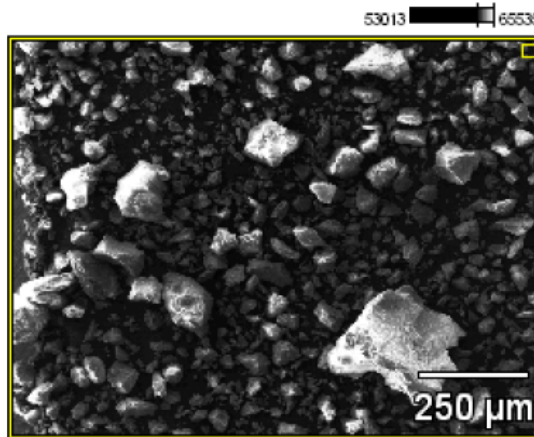


Figure 22.—Joel 75000F scanning electron microscopy (SEM) spectrum of JSC-1a.

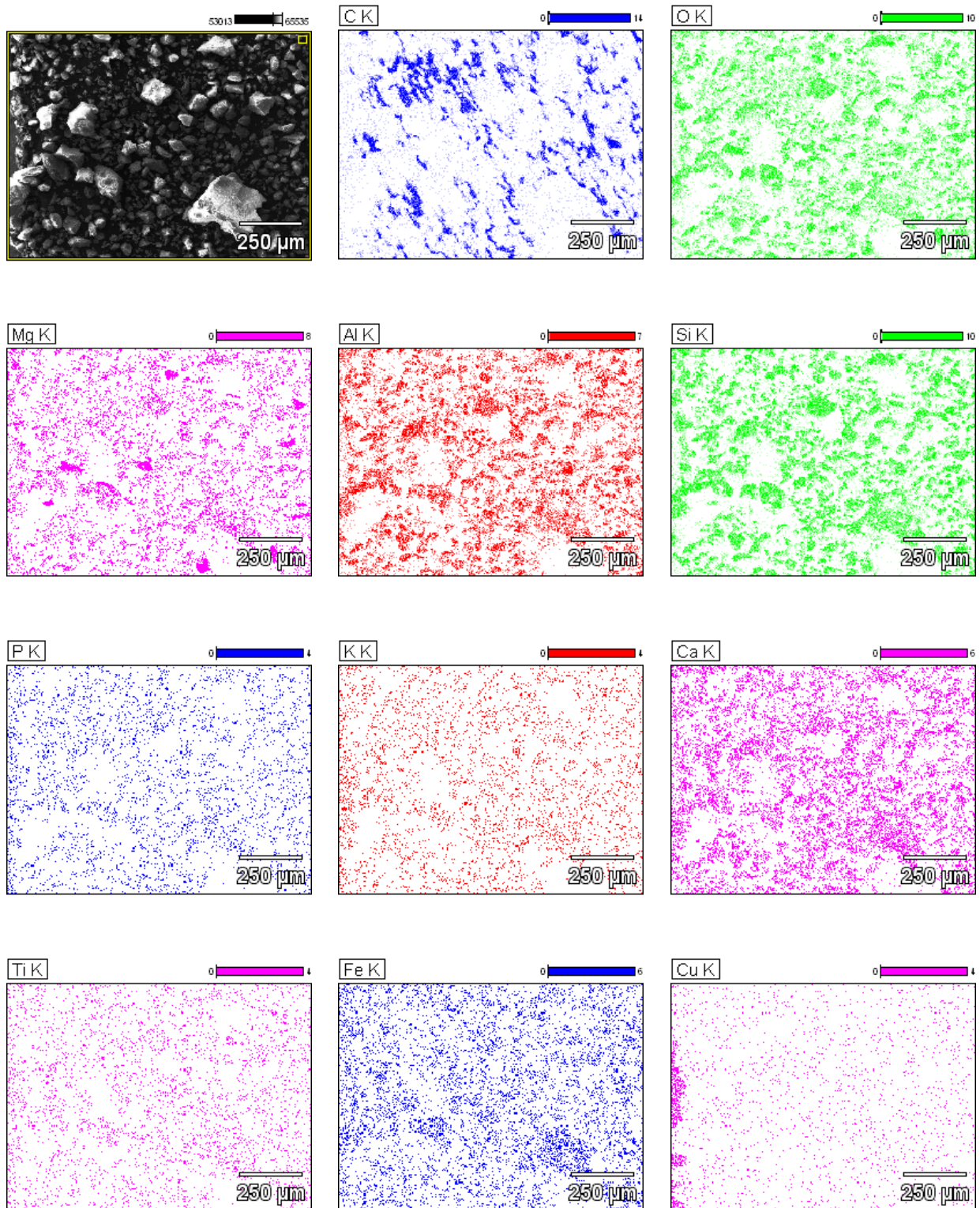


Figure 23.—Energy-dispersive x-ray spectroscopy maps, showing spatial mapping of elements corresponding to scanning electron microscopy (SEM) spectrum of Figure 22.



## Appendix B.—Summary of Particle Shape Considerations

Discrete element method (DEM) simulation software considers a granular material as being made up of a size distribution of idealized particle shapes. These shapes may be simple two-dimensional nonoverlapping or overlapping discs or ellipses, three-dimensional spheres or ellipsoids that overlap or do not overlap, or complex shapes such as polyhedrons or superquadrics. Table IV compares some of the pros and cons of these idealized particle types.

TABLE IV.—COMPARISON OF DISCRETE ELEMENT METHOD (DEM) PARTICLE SHAPE TYPES

Particle shape	Pros	Cons	Comments and possible solutions to cons	Incorporated in DEM software
Sphere	Simplest to implement; requires the minimum CPU <sup>a</sup> resources, allowing a maximum number of simulated particles.	Particle behavior is unrealistic because of simplified shape.	Implements more complex force and friction models to match real particle behavior.	PFC2D/PFC3D (Ref. 5) EDEM (Ref. 6) Yade (Ref. 19)
Rigid nonoverlapping sphere cluster	Relatively simple to implement. Approximates real particle shapes.	In order to approximate a real particle shape, many spheres of various sizes are required, significantly increasing CPU resources.	Decreases number of free-state parameters to only that needed to simulate a single rigid body.	PFC2D/PFC3D (Ref. 5) EDEM (Ref. 6)
Rigid overlapping sphere cluster	Adds ability to better match real particle shapes.	Again, in order to approximate a real particle shape, many spheres of various sizes are required. Some DEM codes (e.g., EDEM) can correctly account for total cluster mass density.	Specifies a variable sphere mass density so that total cluster is the correct value. This increases complexity of sphere density specification.	PFC2D (Ref. 5a)
Ellipsoid	Better matches real particle shapes. Contact force detection has some similarities to that of a sphere. CPU resources required are comparable to that of a sphere.	Contact force detection is more complicated than for a sphere. The ability to match real particles is much better than a sphere, but is still limited. Contact detection is more difficult than for sphere.	Ellipsoid is comparable to rigid sphere cluster as far as tradeoffs between CPU resources, number of possible particles, and similarity of simulated to real particle shape.	Wang (Ref. 21)
Superquadric	More simulated particle parameters are provided in a closed form description, which result in more shapes. All of the particle parameters can be computed analytically.	Similar difficulties encountered as with ellipsoids. When concave exponent values are used ( $n < 2$ ), additional difficulties in contact detection and force model are present.	Because purely analytic methods used for contact detection and force model can get messy, a gridded spatial model of particle and particle interactions may be a better choice.	MIMES (Ref. 17)
Asymmetric superquadric	Similar to superquadric, but many more parameters can be added, providing a better match to real particle shapes.	All problems described for superquadric particle shape are compounded by the inclusion of additional parameters.	Even though an analytical approach to contact detection and force model is possible, it may not be practical in this case. A gridded numerical strategy may be the best approach.	None found

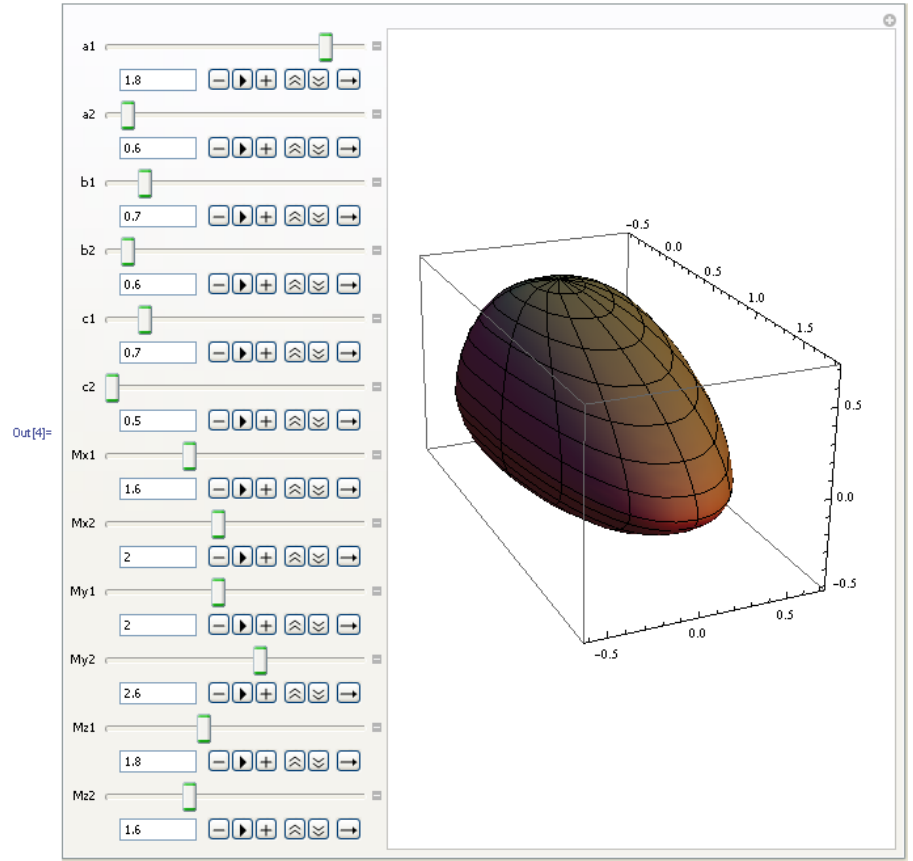
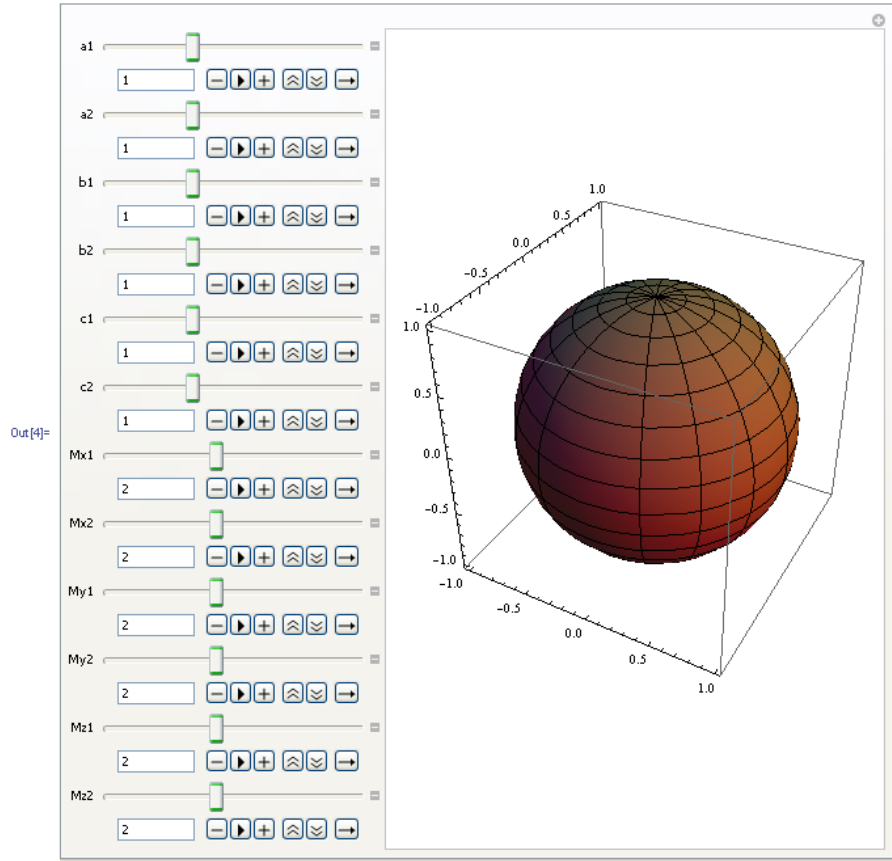
Particle shape	Pros	Cons	Comments and possible solutions to cons	Incorporated in DEM software
Eight-quadrant superquadric	A subset of asymmetric superquadric particle type, which provides a method to easily guarantee no surface discontinuities.	Problems are similar to the asymmetric superquadric.	Gridded representation of particle and particle interactions is probably the most practical approach.	None found
Poly-ellipsoid	A subset of eight-quadrant superquadric particle type, which guarantees no surface gradient discontinuities (i.e., no sharp ridges or edges).	Problems with contact detection are more severe than with the ellipsoid, but less severe than with the general superquadric.	A gridded approach may be best, but other pseudo analytical approaches have been developed which claim good success.	Peters (Ref. 13)
Polyhedra	The polyhedron-based particle shape is the most general shape of those discussed in this summary.	Analytical closed form contact detection methods are very difficult except in specific simple cases. Contact force determination on edges is also difficult and ambiguous.	A gridded approach is almost a necessity. Sharp edges can be eliminated by performing a spatial convolution of the particle surface or volume with a sphere (Minkowski sum, Ref. 22).	Nezami (Ref. 15)

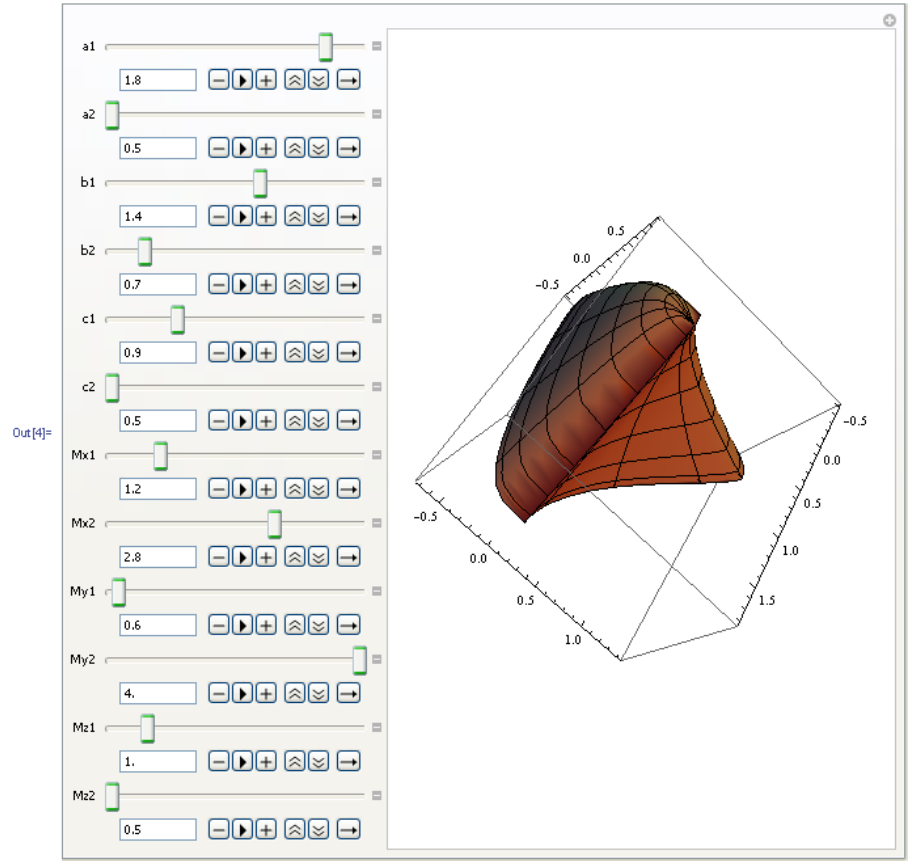
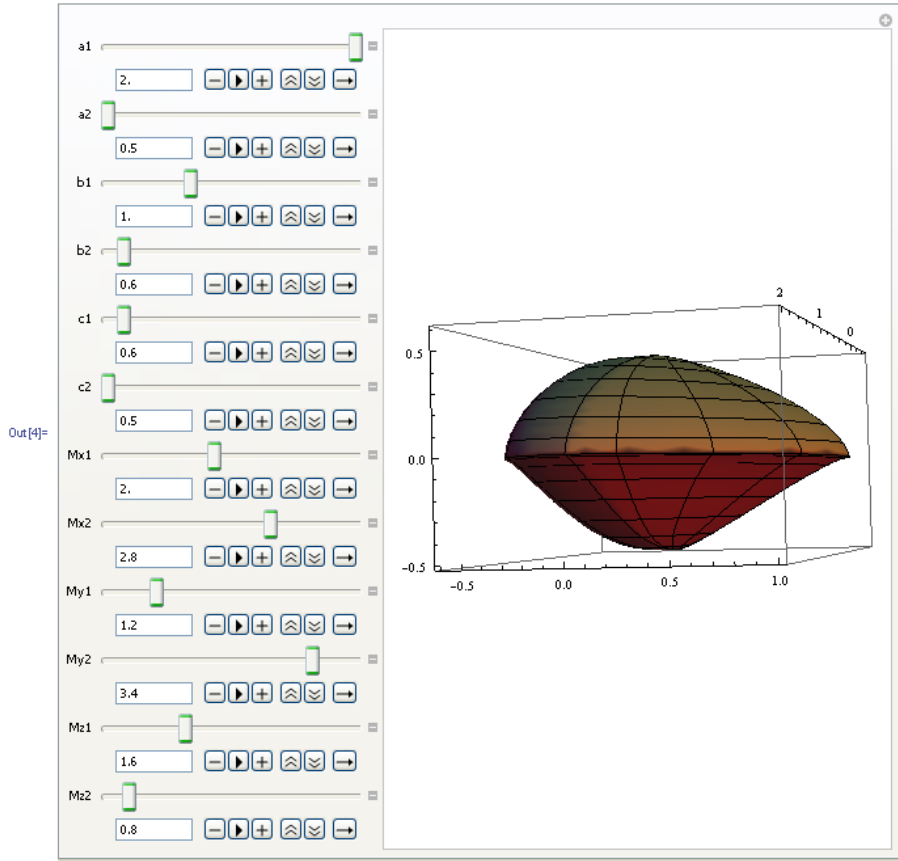
<sup>a</sup>CPU refers to central processing unit.

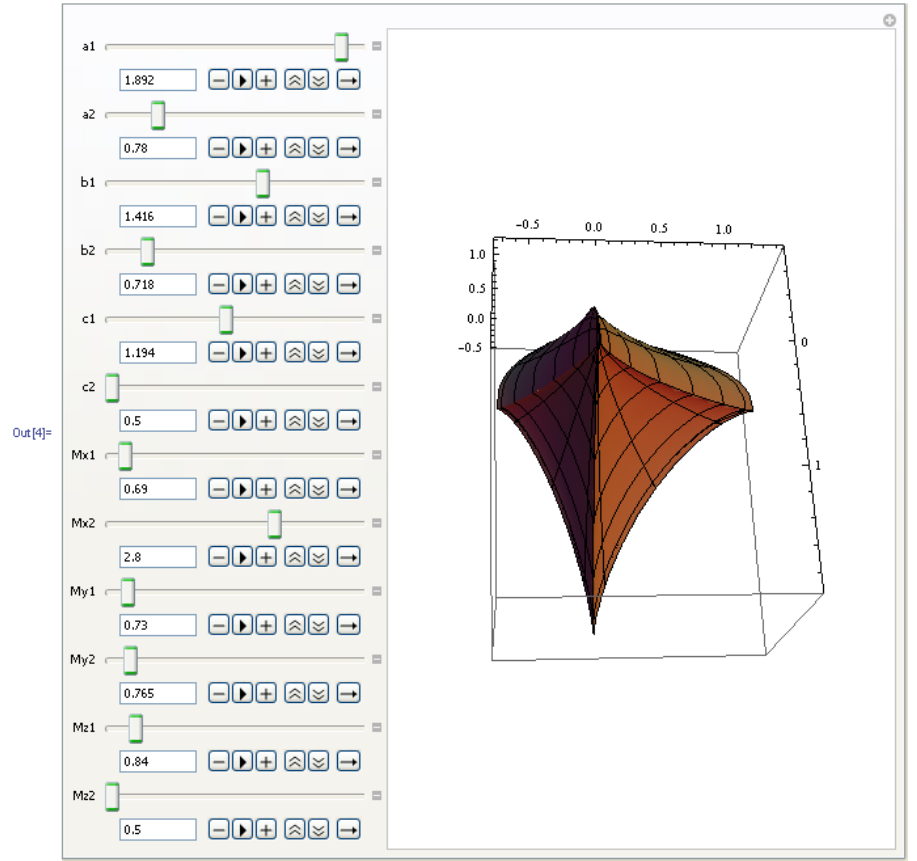
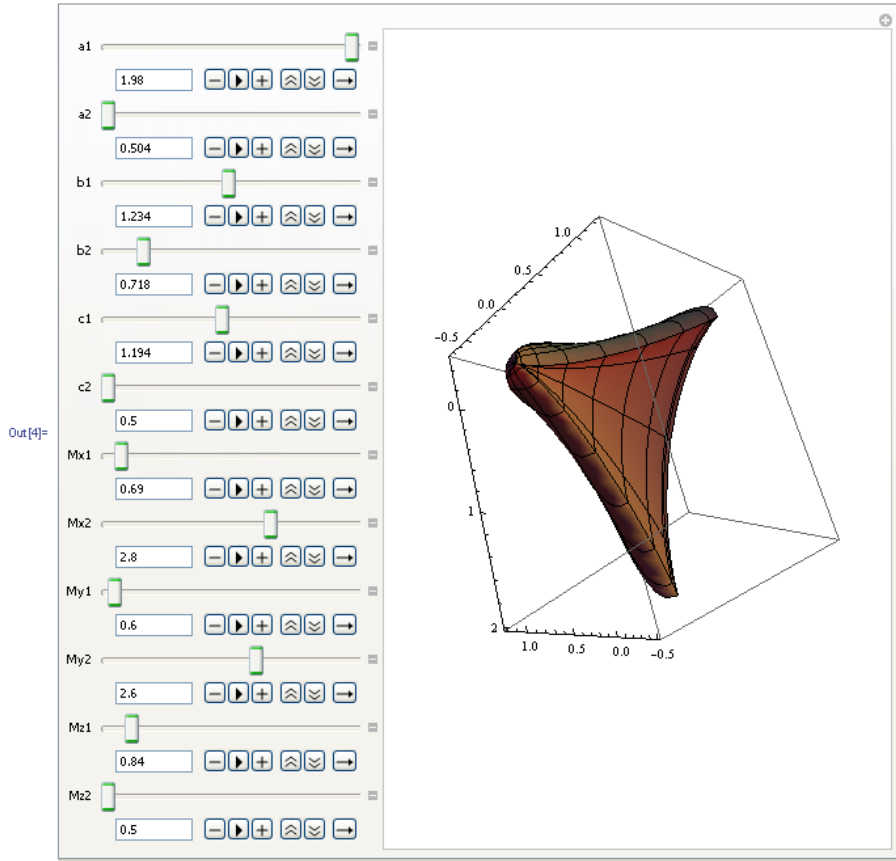
## Appendix C.—Eight-Quadrant Superquadric Particle Shape Examples

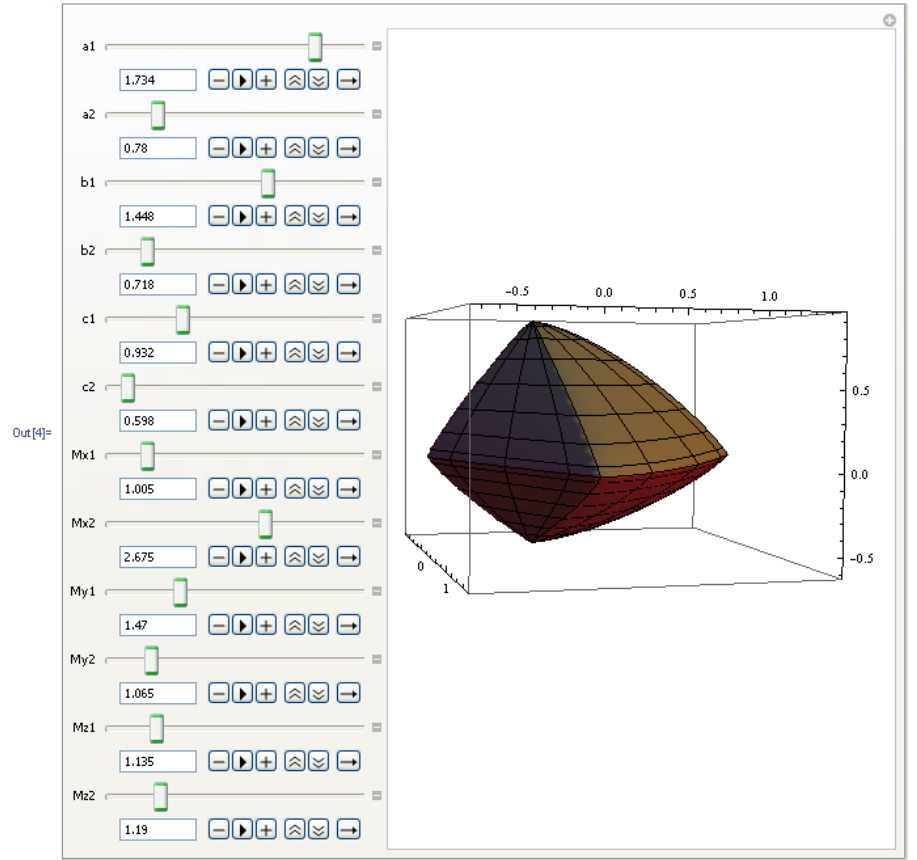
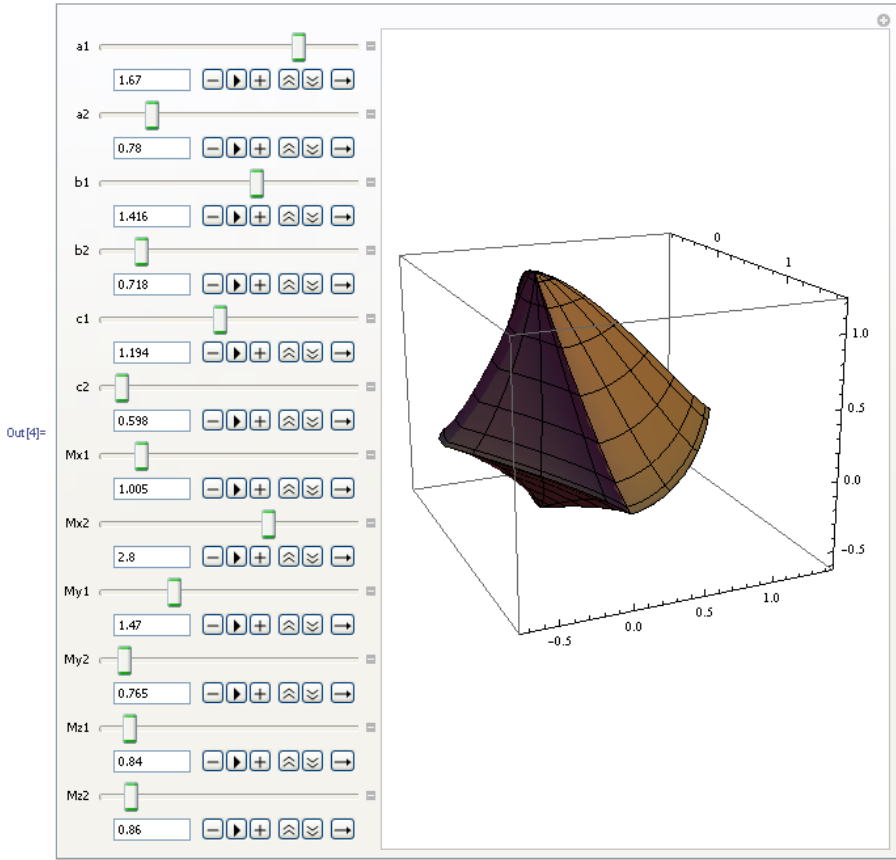
Using Equation (8), the 12 particle shape parameters are randomly modified to demonstrate the resulting diversity of particle shapes. The figures in this appendix were created using Mathematica version 7.0.

$$\begin{aligned}
 x(\theta, \phi) &= \begin{cases} a_1 (\sin \theta \cos \phi)^{2/K_1} & \text{for } -\frac{\pi}{2} \leq \phi < \frac{\pi}{2} \\ a_2 |\sin \theta \cos \phi|^{2/K_2} & \text{for } \frac{\pi}{2} \leq \phi < \frac{3\pi}{2} \end{cases} & 0 \leq \theta < \pi \\
 y(\theta, \phi) &= \begin{cases} b_1 (\sin \theta \sin \phi)^{2/L_1} & \text{for } 0 \leq \phi < \pi \\ b_2 |\sin \theta \sin \phi|^{2/L_2} & \text{for } \pi \leq \phi < 2\pi \end{cases} & 0 \leq \theta < \pi \\
 z(\theta, \phi) &= \begin{cases} c_1 (\cos \theta)^{2/M_1} & \text{for } 0 \leq \theta < \frac{\pi}{2} \\ c_2 |\cos \theta|^{2/M_2} & \text{for } \frac{\pi}{2} \leq \theta < \pi \end{cases}
 \end{aligned} \tag{8}$$











## References

1. Cleary, Paul W.; and Sawley, Mark L.: DEM Modelling of Industrial Granular Flows: 3D Case Studies and the Effect of Particle Shape on Hopper Discharge. *Appl. Math. Model.*, vol. 26, no. 2, 2002, pp. 89–111.
2. Santamarina, J.C.; and Cho, G.C.: Soil Behaviour: The Role of Particle Shape. *Adv. Geotech. Eng. Skempton Conf. Proc.*, 2004, pp. 604–617.
3. Zeghal, M.: Effect of Particle Shapes on the Resilient Behaviour of Aggregate Materials. *Canadian Society for Civil Engineering Annual Conference*, Victoria, 2001, pp. 1–5.
4. Peña, A.A.; García-Rojo, R.; and Herrmann, H.J.: Influence of Particle Shape on Sheared Dense Granular Media. *Granular Matter*, 2007, pp. 279–291.
- 5a. Distinct Element Modeling for Micromechanical Analysis of Geomaterials and Particulate Systems in Two Dimensions. Itasca, Minneapolis, MN, 2010. <http://www.itascacg.com/pfc2d/> Accessed October 12, 2010.
- 5b. Distinct Element Modeling for Micromechanical Analysis of Geomaterials and Particulate Systems in Three Dimensions. Itasca, Minneapolis, MN, 2010. <http://www.itascacg.com/pfc3d/> Accessed October 12, 2010.
6. EDEM Software. DEM Solutions, Edinburgh, Midlothian, 2010. <http://www.dem-solutions.com/software/edem-software.php> Accessed October 12, 2010.
7. Ferrellec, Jean-Francois; and McDowell, Glenn R.: A Method to Model Realistic Particle Shape and Inertia in DEM. *Granular Matter*, vol. 12, no. 5, 2010, pp. 459–467.
8. Ashmawy, Alaa K.; Sukumaran, Beena; and Vinh Hoang, V.: Evaluating the Influence of Particle Shape on Liquefaction Behavior Using Discrete Element Modeling. *Proceedings of the 13th International Offshore and Polar Engineering Conference*, Honolulu, HI, 2003, pp. 1089–1096.
9. Markauskas, D.: Discrete Element Modelling of Complex Axisymmetrical Particle Flow. *Mechanika*, vol. 62, no. 6, 2006, pp. 32–38.
10. Vu-Quoc, L.; Zhang, X.; and Walton, O.R.: A 3–D Discrete Element Method for Dry Granular Flows of Ellipsoidal Particles. *Computer Methods in Applied Mechanics and Engineering on Dynamics of Contact and Impact Problems*, vol. 187, vols. 3–4, 2000, pp. 483–528. <http://clesm.mae.ufl.edu/~vql/pdf/Vu-Quoc2000.pdf> Accessed October 12, 2010.
11. Preece, D.S.; and Perkins, Eric D.: Sand Production Modeling Using Superquadratic Discrete Elements and Coupling of Fluid Flow and Particle Motion. SAND99–0366C, 1999.
12. Wolfram Mathematica 7. Wolfram Research, Champaign, IL, 2010. <http://www.wolfram.com/products/mathematica/index.html> Accessed October 12, 2010.
13. Peters, John F., et al.: A Poly-Ellipsoid Particle for Non-Spherical Discrete Element Method. *Engineering Computations*, vol. 26, no. 6, 2009, pp. 645–657.
14. Zhao, Dawei, et al.: Three-Dimensional Discrete Element Simulation for Granular Materials. *Eng. Comput.*, vol. 23, no. 7, 2006, pp. 749–770.
15. Nezami, Erfan G., et al.: Shortest Link Method for Contact Detection in Discrete Element Method. *Int. J. Numer. Anal. Methods Geomech.*, vol. 30, no. 8, 2006, pp. 783–801.
16. Hogue, Caroline: Shape Representation and Contact Detection for Discrete Element Simulations of Arbitrary Geometries. *Eng. Comp.*, vol. 15, no. 3, 1998, pp. 374–390.
17. Nezami, Erfan G., et al.: Simulation of Front End Loader Bucket—Soil Interaction Using Discrete Element Method. *Int. J. Numer. Anal. Meth. Geomech.*, vol. 31, 2007, pp. 1147–1162. [https://netfiles.uiuc.edu/hashash/www/web/Publications/Nezami\\_etal\\_2007.pdf](https://netfiles.uiuc.edu/hashash/www/web/Publications/Nezami_etal_2007.pdf) Accessed October 12, 2010.
18. Williams, John R., et al.: Dynamic Wave Propagation in Particulate Materials With Different Particle Shapes Using a Discrete Element Method. *Proc. Eng. Mech.*, vol. 1, 1995, pp. 493–496.

19. Yade. 2010. <https://yade-dem.org/wiki/Yade> Accessed October 12, 2010.
20. Bagnold, Ralph Alger: *The Physics of Blown Sand and Desert Dunes*. Dover Publications, Methuen, London, 1954.
21. Wang, Linbing; Park, Jin-Young; and Fu, Yanrong: Representation of Real Particles for DEM Simulation Using X-Ray Tomography. *Constr. Build. Mater.*, vol. 21, no. 2, 2007, pp. 338–346.
22. Alonso-Marroquín, Fernando; and Wang, Yucang: An Efficient Algorithm for Granular Dynamics Simulations With Complex-Shaped Objects. *Granular Matter*, vol. 11, no. 5, 2009, pp. 317–329. <http://www.springerlink.com/content/w58x84mgj8k82083/fulltext.pdf> Accessed October 12, 2010.

REPORT DOCUMENTATION PAGE			Form Approved OMB No. 0704-0188		
<p>The public reporting burden for this collection of information is estimated to average 1 hour per response, including the time for reviewing instructions, searching existing data sources, gathering and maintaining the data needed, and completing and reviewing the collection of information. Send comments regarding this burden estimate or any other aspect of this collection of information, including suggestions for reducing this burden, to Department of Defense, Washington Headquarters Services, Directorate for Information Operations and Reports (0704-0188), 1215 Jefferson Davis Highway, Suite 1204, Arlington, VA 22202-4302. Respondents should be aware that notwithstanding any other provision of law, no person shall be subject to any penalty for failing to comply with a collection of information if it does not display a currently valid OMB control number.</p> <p>PLEASE DO NOT RETURN YOUR FORM TO THE ABOVE ADDRESS.</p>					
<b>1. REPORT DATE (DD-MM-YYYY)</b> 01-12-2010		<b>2. REPORT TYPE</b> Technical Memorandum		<b>3. DATES COVERED (From - To)</b>	
<b>4. TITLE AND SUBTITLE</b> A Review of Discrete Element Method (DEM) Particle Shapes and Size Distributions for Lunar Soil			<b>5a. CONTRACT NUMBER</b>		
			<b>5b. GRANT NUMBER</b>		
			<b>5c. PROGRAM ELEMENT NUMBER</b>		
<b>6. AUTHOR(S)</b> Lane, John, E.; Metzger, Philip, T.; Wilkinson, R., Allen			<b>5d. PROJECT NUMBER</b>		
			<b>5e. TASK NUMBER</b>		
			<b>5f. WORK UNIT NUMBER</b> WBS 387498.04.01.01.02.03		
<b>7. PERFORMING ORGANIZATION NAME(S) AND ADDRESS(ES)</b> National Aeronautics and Space Administration John H. Glenn Research Center at Lewis Field Cleveland, Ohio 44135-3191			<b>8. PERFORMING ORGANIZATION REPORT NUMBER</b> E-17243		
<b>9. SPONSORING/MONITORING AGENCY NAME(S) AND ADDRESS(ES)</b> National Aeronautics and Space Administration Washington, DC 20546-0001			<b>10. SPONSORING/MONITOR'S ACRONYM(S)</b> NASA		
			<b>11. SPONSORING/MONITORING REPORT NUMBER</b> NASA/TM-2010-216257		
<b>12. DISTRIBUTION/AVAILABILITY STATEMENT</b> Unclassified-Unlimited Subject Categories: 31, 59, and 91 Available electronically at <a href="http://gltrs.grc.nasa.gov">http://gltrs.grc.nasa.gov</a> This publication is available from the NASA Center for AeroSpace Information, 443-757-5802					
<b>13. SUPPLEMENTARY NOTES</b>					
<b>14. ABSTRACT</b> As part of ongoing efforts to develop models of lunar soil mechanics, this report reviews two topics that are important to discrete element method (DEM) modeling the behavior of soils (such as lunar soils): (1) methods of modeling particle shapes and (2) analytical representations of particle size distribution. The choice of particle shape complexity is driven primarily by opposing tradeoffs with total number of particles, computer memory, and total simulation computer processing time. The choice is also dependent on available DEM software capabilities. For example, PFC2D/PFC3D and EDEM support clustering of spheres; MIMES incorporates superquadric particle shapes; and BLOKS3D provides polyhedra shapes. Most commercial and custom DEM software supports some type of complex particle shape beyond the standard sphere. Convex polyhedra, clusters of spheres and single parametric particle shapes such as the ellipsoid, poly-ellipsoid, and superquadric, are all motivated by the desire to introduce asymmetry into the particle shape, as well as edges and corners, in order to better simulate actual granular particle shapes and behavior. An empirical particle size distribution (PSD) formula is shown to fit desert sand data from Bagnold. Particle size data of JSC-1a obtained from a fine particle analyzer at the NASA Kennedy Space Center is also fitted to a similar empirical PSD function.					
<b>15. SUBJECT TERMS</b> Geotechnical engineering; Particle size distribution; Lunar soil; Shapes; Discrete modeling					
<b>16. SECURITY CLASSIFICATION OF:</b>			<b>17. LIMITATION OF ABSTRACT</b>  UU	<b>18. NUMBER OF PAGES</b>  35	<b>19a. NAME OF RESPONSIBLE PERSON</b> STI Help Desk (email: <a href="mailto:help@sti.nasa.gov">help@sti.nasa.gov</a> )
<b>a. REPORT</b> U	<b>b. ABSTRACT</b> U	<b>c. THIS PAGE</b> U			<b>19b. TELEPHONE NUMBER (include area code)</b> 443-757-5802



